Korean J. Chem. Eng., 40(9), 2219-2238 (2023)
DOI: 10.1007/s11814-022-1355-1

pISSN: 0256-1115
eISSN: 1975-7220

Rhodamine B dye degradation by fabricated Ti/RuO_2 anode: Optimization by RSM, reaction mechanism, study of sludge

Monica Ranga, Shishir Sinha†, and Pinakshi Biswas

Department of Chemical Engineering, Indian Institute of Technology Roorkee, Roorkee 247667, Uttarakhand, India
(*Received 16 August 2022 • Revised 19 November 2022 • Accepted 23 November 2022*)

Abstract−Textile wastewater was treated by an electrochemical process using Ti/RuO_2 as anode and stainless steel as a cathode. Textile wastewater contains harmful dyes that can be broken down into simpler products like CO_2 and H_2O using the electro-oxidation process. For this process, a dimensional stable anode (Ti/RuO_2) was fabricated using sol-gel method. Apreo field emission scanning electron microscopy (FE-SEM) with energy dispersed x-ray (EDX), atomic force microscopy (AFM), X-ray diffraction (XRD) has been done to study their characteristics. Design expert software was used to optimize the parameters using response surface methodology. Response parameters such as pH (2-10), current (0.5-2 A), initial concentration (50-200 mg/L), and time (2-15 min) were varied, and 30 sets of experiments were designed. The optimized value obtained for maximizing the dye degradation percentage and COD removal percentage is at initial pH of 3.3, current of 0.5 A, initial concentration of 50 mg/L, and time of 9.4 min for dye degradation of 99.82%, COD removal of 82.50% removal, and 1.81 kWh/m^3 energy consumption (minimum) keeping 0.2 M NaCl electrolyte as constant. Kinetic study shows that the reaction is first order. The mechanism of the process was also studied using UPLC-QTOF. The total cost of the process was found to be ₹582.79 or $7.68. Characterization of the sludge was also done to check its reusability.

Keywords: Ti/RuO_2 Anode, Response Surface Methodology, Reaction Mechanism, Cost Analysis

INTRODUCTION

The textile industry is an important part of industrial development worldwide. India is the third largest producer of textiles after China and the European Union [1]. But the problem is the large amount of wastewater effluent production in the dyeing unit of the industry that contains color and toxic compounds that are harmful to the marine species. Therefore, there is a crucial need for its treatment. Textile wastewater can be treated through many conventional methods like biological treatment, adsorption, chemical coagulation, ozonation, and the Fenton process. Many other methods, such as adsorption of the dyes by using hydrogels, are being used. Jiao et al. [2] prepared self-assembled reduced graphene oxide (RGO)/chitosan/silver nanoparticle composites for dye degradation. Similarly, Ma et al. [3] developed graphene oxide-modified Fe_3O_4 magnetic nanoparticles with doping of sodium alginate/chitosan gel for degradation of cationic dye. Yin et al. [4] developed a novel polyvinyl alcohol/polyacrylic acid membrane for wastewater treatment. Yet, these methods are inadequate in terms of cost-effectiveness or inability to treat the complete composition of the textile effluent [5]. Nowadays, electrochemical treatment is being used as it is robust, flexible, easy to operate, time saving, economically feasible, and can be used for both organic and inorganic treatment of industrial wastewater such as phenolic wastewater [6], food processing industry [7], tannery industry [8], and nitrate-containing wastewater [9].

Conventionally, iron, lead, copper, aluminum, stainless steel, graphite, and various alloys have been used as anodes for wastewater treatment, but corrosion, mechanical wear, releasing impurities, and the loss of geometric shape (not stable) limit their usage. Zhang et al. [10] fabricated Sn/Mo_2C-CNFs carbon-based electrocatalyst that has relatively low cost and shows better efficiency, but these are not highly stable. Fe_2O_3 is considered to be a highly conductive compound that has been used classically as anode material, but these iron oxides change their volume and decay in a few cycles of usage [11]. To overcome these problems dimensional stable anode (DSA) is used that preserve the shape and structural integrity of the material. DSAs are anodes with Ti as a base having metal oxide coating. These have exceptional stability. Different DSAs such as Ti/Pt [12], Ti/IrO_2 [13], Ti/SnO_2 [14], Ti/Sb/SnO_2 [15], and BDD [16] are used for electrochemical treatment of the wastewater. But we used Ti/RuO_2 anode due to its stability, service life, and low cost compared to the other anodes. Among the other fabrication methods of the anodes, the advantages of the sol-gel method [17] include mild reaction conditions, stability of the structure, and chemical composition of the anode. It can control chemical kinetics. This method enables the preparation of a multi-component layer, and even the small amount of dopant in the sol gets distributed uniformly [18]. Response surface methodology (RSM) [19-22] provides an organized and efficient research strategy to detect the interactive effects of many parameters using statistical procedures [23]. It includes reduced costs, requiring fewer tests, and time-saving [24].

This study prepared low-cost Ti/RuO_2 anodes using sol-gel method and treated textile wastewater using these anodes while optimizing the treatment process by the response surface method using a central composite design. This methodology, Fe-SEM, XRD, AFM,

†To whom correspondence should be addressed.
E-mail: shishir@ch.iitr.ac.in
Copyright by The Korean Institute of Chemical Engineers.

and XPS of the Ti/RuO_2 anode and stainless-steel cathode, has been done to study their characteristics. The electrochemical properties and the stability of the Ti/RuO_2 have been studied using cyclic voltammetry (CV). Polyester textile wastewater was collected from the dyeing unit of the textile industry in Panipat, India and characterization was done before and after its treatment of one sample, but real wastewater changes its characteristics daily. To avoid the complexity in optimization of the process parameters, we have taken Rhodamine, which is being used for dyeing of polyester fabric in the industry. Reaction kinetics and mechanistic studies have been done to know the reaction process. A total cost analysis of the process has also been done. Further sludge composition has been studied in our work to understand its reusability.

MATERIALS AND METHOD

1. Chemicals or Materials Used

All chemicals used for the experimental work were of analytical grade. LC/MS grade acetonitrile (C_2H_3N), formic acid (CH_2O_2), and methanol (CH_3OH) were used for wastewater analysis. Citric acid anhydrous ($HOC(CH_2CO_2H)_2$), ethylene glycol ($(CH_2OH)_2$), and oxalic acid dihydrate ($C_2H_2O_4{\cdot}2H_2O$) used were from Avantor Performance Materials India Limited. Sodium hydroxide Pellets were from Chemigens Research and Fine Chemicals. Rhodamine B dye was purchased from Sigma-Aldrich. All stock solutions were made from double distilled water. Titanium sheets were purchased from Italy. A stainless-steel sheet was purchased from Teesla pvt ltd. RuO_2 was purchased from TCI Chemicals (India) Pvt. Ltd.

2. Properties of Rhodamine B Dye

Rhodamine B dye is a water soluble fluorescent xanthene dye used in the textile industry for dyeing various substances. It has a molecular weight of 479.02 with the chemical formula $C_{28}H_{31}ClN_2O_3$ and melting point 210-211 °C. Its solubility in water varies from 8-15 gL^{-1} at 20 °C. It has a maximum absorption wavelength of 554 nm and a maximum emission wavelength of 625 nm. It has a color index of 45170 with a chemical structure that is shown in the mechanism part in Fig. 13.

3. Preparation/Fabrication of the Anode

3-1. Pre-treatment of the Substrate

Ti (5.5×4×0.1 cm) was used as the substrate of the RuO_2 polymeric blend coating. The substrate was first sandblasted with 400 mesh sandpaper. It was initially degreased at 80 °C in 40% NaOH for 30 min. Then ultrasonic cleaning was done by immersing it in the concentrated HCl for 5 min. Finally, it was etched in 10% oxalic acid solution for 2 h. The weight of the pre-treated electrode was measured and found to be 4.1562 g.

3-2. Precursor Solution

Citric acid, ethylene glycol, and $Rucl_3$ were taken in 0.76: 3.52: 0.25 ratio. First, 2.144 ml of ethylene glycol was heated at 60 °C. Then 1.4601 g of the citric acid was added slowly with continuous stirring until the mixture was obtained, followed by increasing the temperature to 90 °C. Finally, 0.518 ml of $RuCl_3$ was added to the mixture and stirred for 20 min [25].

3-3. Coating Method

The precursor solution was coated with a brush and treated for 30 min at 130 °C, followed by heating at 250 °C for 10 min to increase the adherence. It was calcined at 450 °C for 5 min to remove volatile matters and convert chloride to oxide [26]. The measured weight was 4.1730 g after coating the first layer. This procedure was repeated nine times for the building of nine layers. An increase in the weight of the electrode after each layer is shown in the supplementary data (Table S1). Finally, calcination at 400 °C in the air atmosphere for 1 h was done for complete decomposition into oxide.

4. EC Reactor and Operational Procedure

All experiments were done in batch mode. A glass beaker with dimensions 9 cm×7 cm (diameter) was used as a wastewater container. A magnetic stirrer with a temperature controller was used for continuous mixing with a speed up to 1,200 rpm. DC power supply (Baba Gurditta Corporation Limited) with voltage (0-30 V) and current (0-10 A) control was used. A digital pH meter (Labman Scientific Instrument) was used for pH measurement. pH was varied using dilute NaOH and HCl solutions. Ti/RuO_2 electrode prepared with the dimensions of 5.5×4×0.1 cm was used as the anode, and stainless steel of the exact dimensions was used as the cathode. The setup is pictured in Fig. S1 of supplementary data.

200 mL of the dye solution was taken in a 250 mL beaker, and 0.2 M NaCl was used as an electrolyte. The wastewater was stirred continuously at 300-350 rpm speed. The variation of the parameters was studied using RSM. The current was varied from 0.5-2.0 A, pH from 2-10, electrolysis time from 2-15 min, and initial concentration from 50-200 mg/L [27]. The initial and the final range of the parameters are given in the coded form in Table 2. The setup was maintained at a constant room temperature of 25±5 °C.

5. Instrumentations and Analytical Method

The concentration of the samples was calculated using a Shimadzu UV-1800 UV-Vis spectrophotometer at 554 nm wavelength. COD was measured using a COD analyzer using the standard method. The acquired sample information was analyzed in UNIFI software (from Waters). The analyses were completed using a UPLC (Waters Acquity) coupled with QToF (Waters Xevo G2-XS). The UPLC was equipped with a reversed phase C18 column (Acquity UPLC BEH C18 1.7 μm, 2.1×150 mm). The column was operated at 50 °C, while the samples were maintained at 15 °C. Water with 0.1% formic acid (mobile phase A) and acetonitrile with 0.1% formic acid (mobile phase B) were used as mobile phases. 12 min gradient program with a constant flow rate of 0.4 ml/min was used to achieve chromatographic separation. The gradient started with 80% of mobile phase A, held up to 0.5 min, then gradually changed to 10% of mobile phase A at 9 min. At 11 min, the composition of mobile phase A was again brought back to 80%, which was held up to 12 min. All the samples were analyzed in ESI positive. Argon gas was used as collision gas, while nitrogen gas was used as nebulizing gas. The capillary and cone voltages were equal to 3 kV and 40 V, respectively. The high collision energy varied between 20 to 30 eV. The HRMS scans were performed for m/z 50-1200 with a continuous infusion of 200 ng/mL of leucine-enkephalin to maintain high mass accuracy. The acquired data were further analyzed with Empower software (Waters).

THEORY AND CALCULATIONS

The percent degradation of the dye wastewater was measured

by UV/Vis spectrophotometer. A calibration curve at wavelength λ_{max}=554 nm [28] was drawn, which relates the absorbance and the concentration according to the Beer-Lambert law [29],

$$A=\varepsilon lC \tag{1}$$

where A is the absorbance, ε is the extinction coefficient, which is sample specific, l is the optical path length, and C is the concentration of the sample. Percent degradation can be calculated using the formula,

$$\text{Degradation efficiency (\%)}=\frac{C_o-C_t}{C_o}\times 100 \tag{2}$$

where C_o is the initial concentration of the dye, C_t is the concentration at time t of the dye. Overall oxidation of the wastewater can be calculated by COD measurement using the digestion method. COD efficiency can be calculated using the following relation:

$$\text{COD removal efficiency (\%)}=\frac{COD_o-COD_t}{COD_o}\times 100 \tag{3}$$

where COD_o is the initial COD, COD_t is the COD at time t. The energy consumption in kWh/m^3 was calculated using the following formula:

$$\text{Energy consumption}=\frac{U_{cell}it}{3{,}600V} \tag{4}$$

where U_{cell} (V) is the potential voltage of the electrochemical cell, i (A) is the current, t (min) is the electrolysis time, and V (mL) is the volume of the wastewater.

To calculate the reaction kinetics, rate equations were used to determine the best fitted model. I_{st} order equation and nth order power law were applied to find the best model [30,31]. The expressions used for these models are as follows:

1st order model

$$-\frac{d[C]}{dt}=kC \tag{5}$$

Solving the above equation,

$$\ln\frac{C_o}{C_t}=kt \tag{6}$$

n_{th} order model

$$-\frac{d[C]}{dt}=k_nC^n \tag{7}$$

Solving,

$$\frac{1}{C_t^{n-1}}-\frac{1}{C_o^{n-1}}=(n-1)kt \tag{8}$$

Rearranging the above equation and taking the log, it becomes as follows:

$$\ln t=-\ln k(n-1)+(n-1)\ln\left(\frac{C_o}{C_t}\right) \tag{9}$$

where C is the concentration, k (min^{-1}) is the rate constant for the first order, and k_n (mmol^{-1})$^{(1-n)}$ (min^{-1}) is the rate constant for the nth order. C_o and C_t are the concentrations at time 0 and t, respectively.

Non-linear least squares were applied for calculating the order and rate constant of the nth order reaction and to minimize the error. Polymath and origin software was used for calculating these terms. The average relative error was found using the following equation [32]:

$$ARE(\%)=\frac{100}{N}\Sigma_{j=1}^{n}\left[\frac{(C_t)_{exp}-(C_t)_{cal}}{(C_t)_{exp}}\right]_j \tag{10}$$

where $(C_t)_{exp}$ and $(C_t)_{cal}$ are the experimental concentration and the calculated concentration by the fitted equation.

RESULTS AND DISCUSSION

1. X-Ray Diffraction (XRD)

The XRD spectrum of both the anode and cathode is represented in Fig. 1, where (a) shows the presence of the rutile Ti (ICSD reference number 98-009-2049) and RuO_2 (ICSD reference number 98-005-6127) with hexagonal and tetragonal structures, respectively, of the Ti/RuO_2 anode. The diffraction peaks of Ti at an angle 2θ= 5.097,38.412, 53.009, and 70.660 with reflection plane (010), (002), (012), and (013), respectively, have intensity of 250, 273, 135 and 180, respectively, before treatment and after treatment has intensity of 241, 257, 128 and 149. Fig. 1(b) shows the XRD of cathode stainless steel (Fe, Mn, Ni, Cr) and iron oxide [33,34]. Due to decreased intensity, the crystallinity of the anode surface also decreases because during the reaction anode surface loses ions.

2. Scanning Electron Microscopy (SEM)

The morphology of the electrodes is described by the FE- SEM images in Fig. 1. Freshly prepared TiO_2 shows a homogeneous surface [35] and spherical lumps morphology at higher magnification, as shown in Fig. 1((c) and (e)). After the anode was used several times, its surface showed cracks, and pits. It shows that the metal oxide layer of the anode gets fissures with the increase in its usage for electrochemical treatment. Fig. 1((g) and (h)) shows the morphology of the stainless-steel cathode. Before the treatment process, the cathode has a homogeneous structure. After the EC treatment process, its image shows the holes with rocks type structure (Fig. 1(h)), i.e., its structure became heterogeneous. EDX analysis and elemental mapping of both anode and cathodes are shown in Fig. 2. Fig. 2(a) and (b) show the presence of Ti, Ru, and O in the anode before the treatment and after treatment Cl is also present because of the electrolyte NaCl. Their atomic and weight percent can also be seen in Fig. 2. Fig. 2(c) and (d) show Fe, Cr, Ni, Mn, O, and Cl in the stainless steel cathode for before electrochemical treatment and after treatment.

3. Atomic Force Microscopy (AFM)

It is a topographical study of the electrodes. 2D and 3D images of Ti/RuO_2 [36] anode and stainless steel cathode [37] before and after electrochemical treatment are shown in Fig. S2 and 5. Surface roughness can be seen by histogram analysis of both anode and cathode in Fig. 5((e) and (f)). The average surface roughness (S_a) of both anode and cathode increases after the electrochemical reaction. It was found to be 96.9075 nm and 119.421 nm before and after treatment, respectively, for Ti/RuO_2 anode. For stainless steel, S_a was found to be 85.3376 nm and 145.76 nm before and after

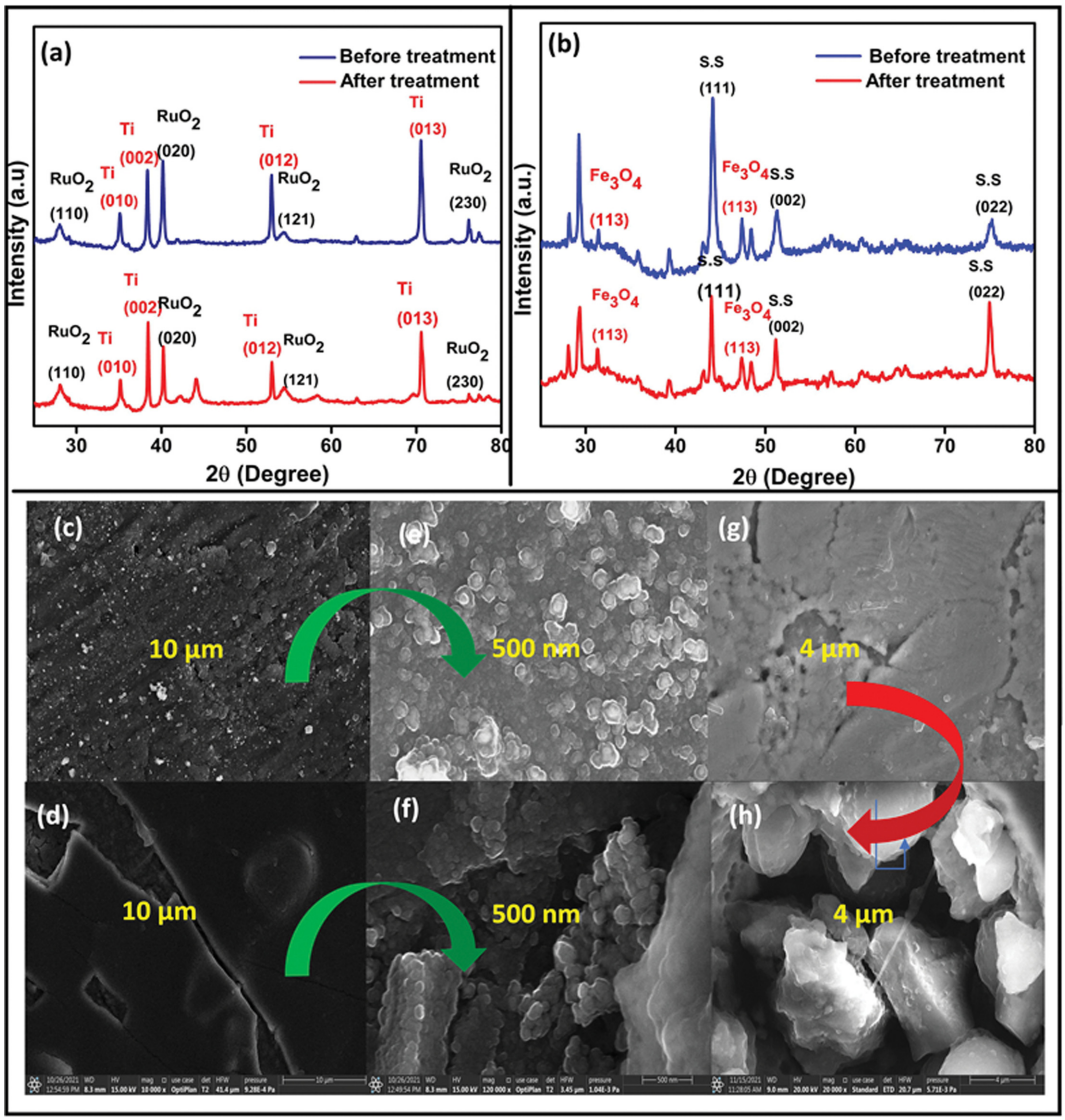


Fig. 1. XRD patterns of the (a) Ti/RuO_2 anode, (b), Stainless steel cathode, FE-SEM of the (c), (e) Ti/RuO_2 anode before and (d), (f) after treatment process (g) and (h) S.S. cathode of before and after treatment process at different micron magnification.

their electrochemical treatment. It might be due to the electron transfer from anode to cathode in the whole process. Metal ion gets released from the anode, and a redox reaction happens at the anode and cathode. Cross-section analysis is shown in supplementary file Fig. S2(a)-(d).

4. X-ray Photoelectron Spectroscopy (XPS)

To study the valence state and elemental composition, XPS was employed for Ti/RuO_2 anode and stainless steel cathode for fresh electrode and after treatment process electrode. Fig. 3(a) shows the presence of Ru 3d, Ti 2p, and O 1s. Ru 3d spin orbital spectrum is shown in Fig. 3(c) with Ru 3d5/2 and Ru 3d3/2 at their binding energies of 280.10 eV and 284.40 eV, respectively [38-42]. In Ru 3d5/2 spin orbital, the oxidation state of Ru is Ru^{+3} at 280.10 eV and Ru^{+6} at 281.90 eV binding energies, respectively. Ru 3d3/2 spin orbital oxidation state changes from Ru^{+2} to Ru^{+4} at their binding energy of 284.40 eV and 285.7 eV. Their respective composition changes from 45.86% to 17.39 for Ru^{+2} oxidation state and 30.31% to 47.95% for Ru^{+4} oxidation state after the treatment process. This implies that electrons were transferred from Ru^{+2} to Ru^{+4} oxidation and the Ru^{+4} atom's composition percentage increased after the treatment process. XPS spectra of O 1s are depicted in Fig. 3(d) for the before-treated anode and the after-treated anode. After deconvolution, three peaks can be seen at binding energies 529.40 eV, 531.20 eV, and 534.10 eV, which could be assigned to lattice oxygen, surface adsorbed oxygen, adsorbed carbonates, and molecular water. At the anode, lattice oxygen with a composition of 30.57% and surface adsorbed oxygen with a composition of 30.64% before the treatment process changed to 19.54% and 73.56% after electrochemical treatment [43]. That means lattice oxygen was reduced to oxidize Ru^{+2}/Ru^{+4}. The valence shell elemental composition of S.S cathode is shown in Fig. 3(b) before and after the electrochemical process.

5. Cyclic Voltammetry

The electrochemical tests were performed using CV (AUTOLAB-

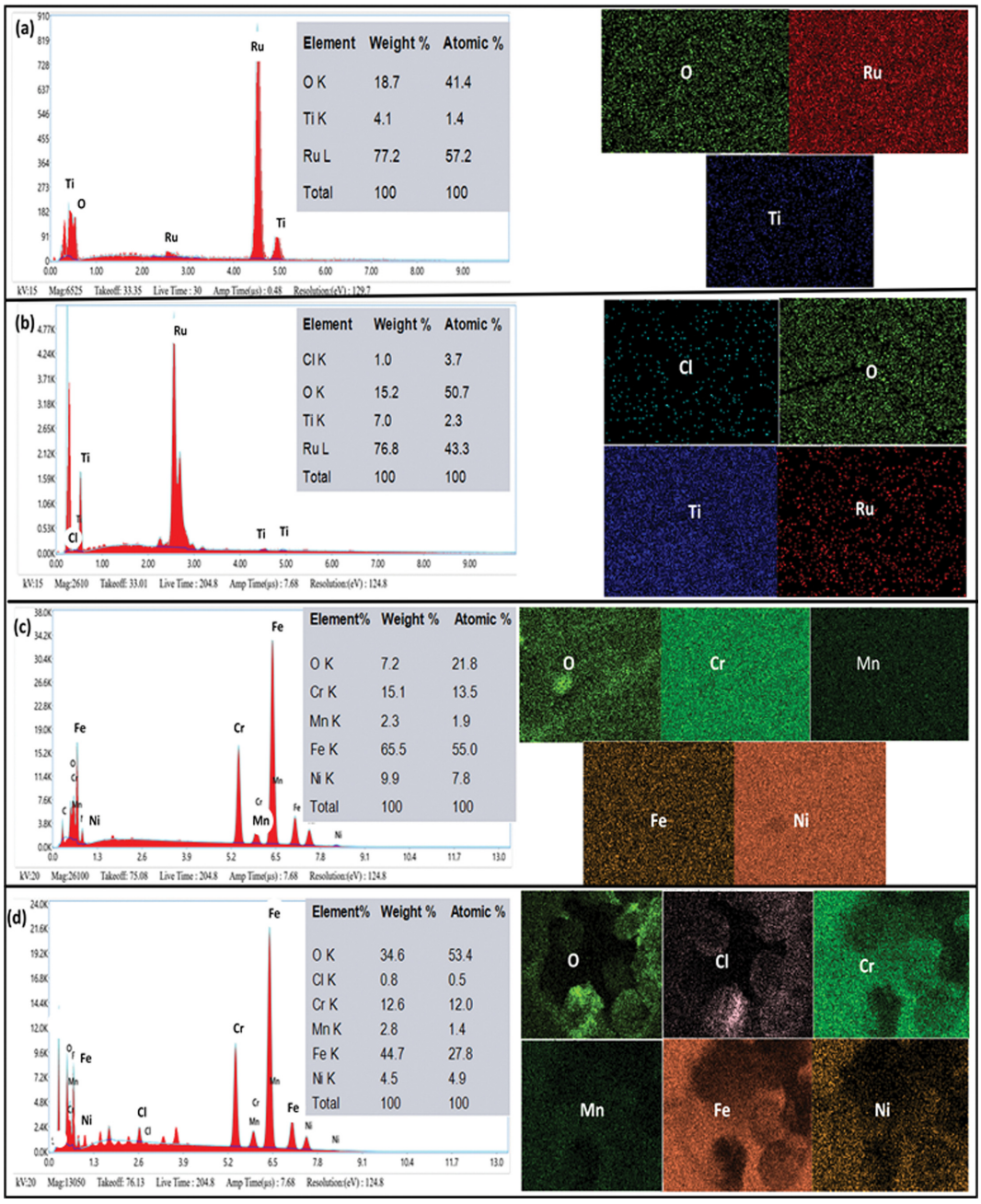


Fig. 2. EDX of Ti/RuO_2 (a) before treatment (b) after treatment and S.S., (c) before treatment, (d) after treatment.

PGSTAT 101) for studying the electrochemical behavior and the stability of the anode. All CV tests were performed at the scanning rate of 1 V s^{-1} and 0.1 M Na_2SO_4 was used as the electrolyte solution. The CV curves are shown in Fig. 4((a) and (b)). The oxidation peak appeared at 0.05 V in the solution and reduction peak can be seen at 0.98 V, which is greater than the commercial electrode used by [32]. This curve shows that the redox reaction is happening in the electrochemical cell. Moreover, for measuring the stability of the Ti/RuO_2, 300 scan laps were performed in the electrochemical workstation with a scanning range of −1 V to 1 V, and the curves of 1st lap and 300th lap were plotted as depicted in Fig. 4(b). the 1st lap coincides with the 300th lap, which shows that this anode can be used 300 times without changing the electrochemical properties, indicating greater stability of the Ti/RuO_2 during the electrochemical process [44].

6. Experimental Design through RSM

RSM is a mathematical/statistical tool that relates the input variables with response variables for empirical model building for industrial processes. RSM provides better result reproducibility and optimized responses using a set of designed experiments. In RSM, response surfaces are represented in graphs between the independent input process variables and the output responses. Central composite design [45-47] is the most popular, efficient, and flexible factorial design that gives more information on the overall experi-

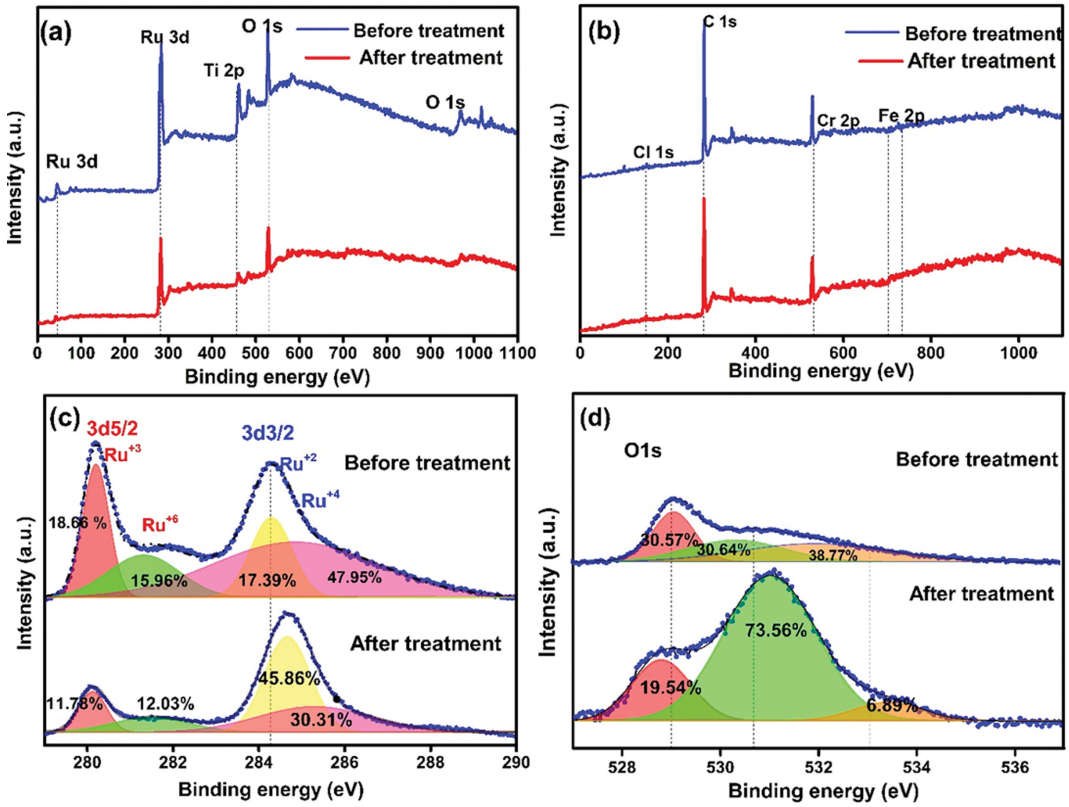


Fig. 3. XPS spectrum for (a) Ti/RuO_2 anode, (b) S.S cathode, (c) core level spectrum of Ru 3d, (d) core level spectra of O 1s.

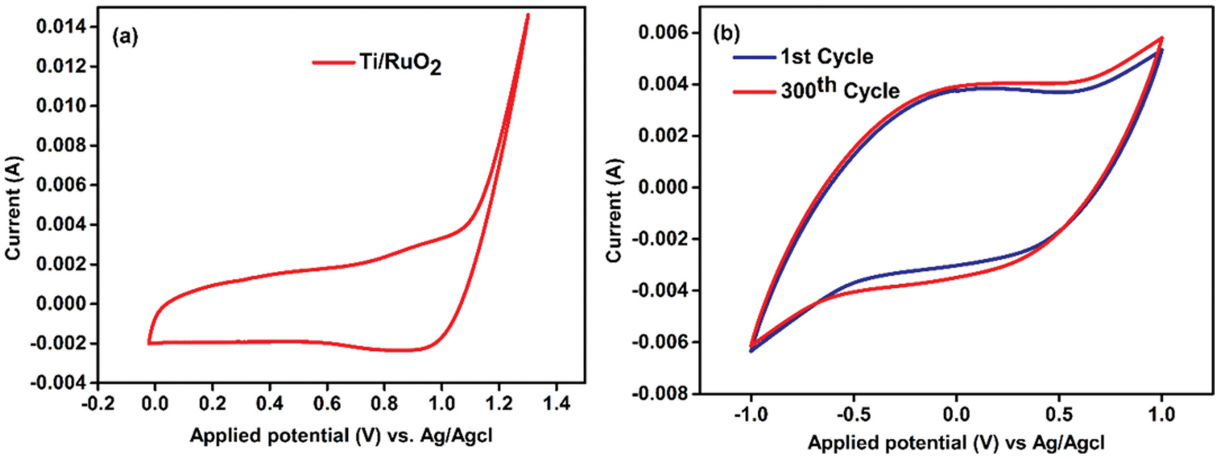


Fig. 4. CV curves of (a) Ti/RuO_2 at the scanning range of 0.2 V to 1.3 V and scanning speed of 1 V s^{-1} (b) stability of the Ti/RuO_2 at scanning range of −1 V to 1 V and scanning speed of 1 V s^{-1}.

mental error and the variable effects in minimum requisite runs by evaluating through a rationalized number of design points [48].

Optimization of the process involves coefficients estimation, response prediction, and inspection of the acceptability of the model [49]. The relationship between the independent variable and the response is represented in Eq. (11):

$$Y=f(X_1, X_2, X_3, \ldots\ldots\ldots\ldots X_n)\pm E \quad (11)$$

where f is the response function, Y is the response, X_1, X_2,…….X_n are the independent input variables, and E is the experimental error.

The polynomial equation of the second-order quadratic model (equation) is represented below:

$$Y=\beta_o+\Sigma_{i=1}^{k}\beta_i X_i+\Sigma_{i=1}^{k}\beta_{ii}X_i^2+\Sigma\Sigma_{i<j}\beta_{ij}X_iX_j+E_r \quad (12)$$

where Y is the response, β_0 is the regression coefficient, β_i, β_{ii} and β_{ij} are the linear, quadratic, and the interaction coefficient, respectively. X_i, X_j, is the process variable's coded values, and the E_r is the residual error value.

Performance factors such as coefficient of determination (R^2) and adjusted coefficient of determination (R^2_{adj}) for accuracy of the

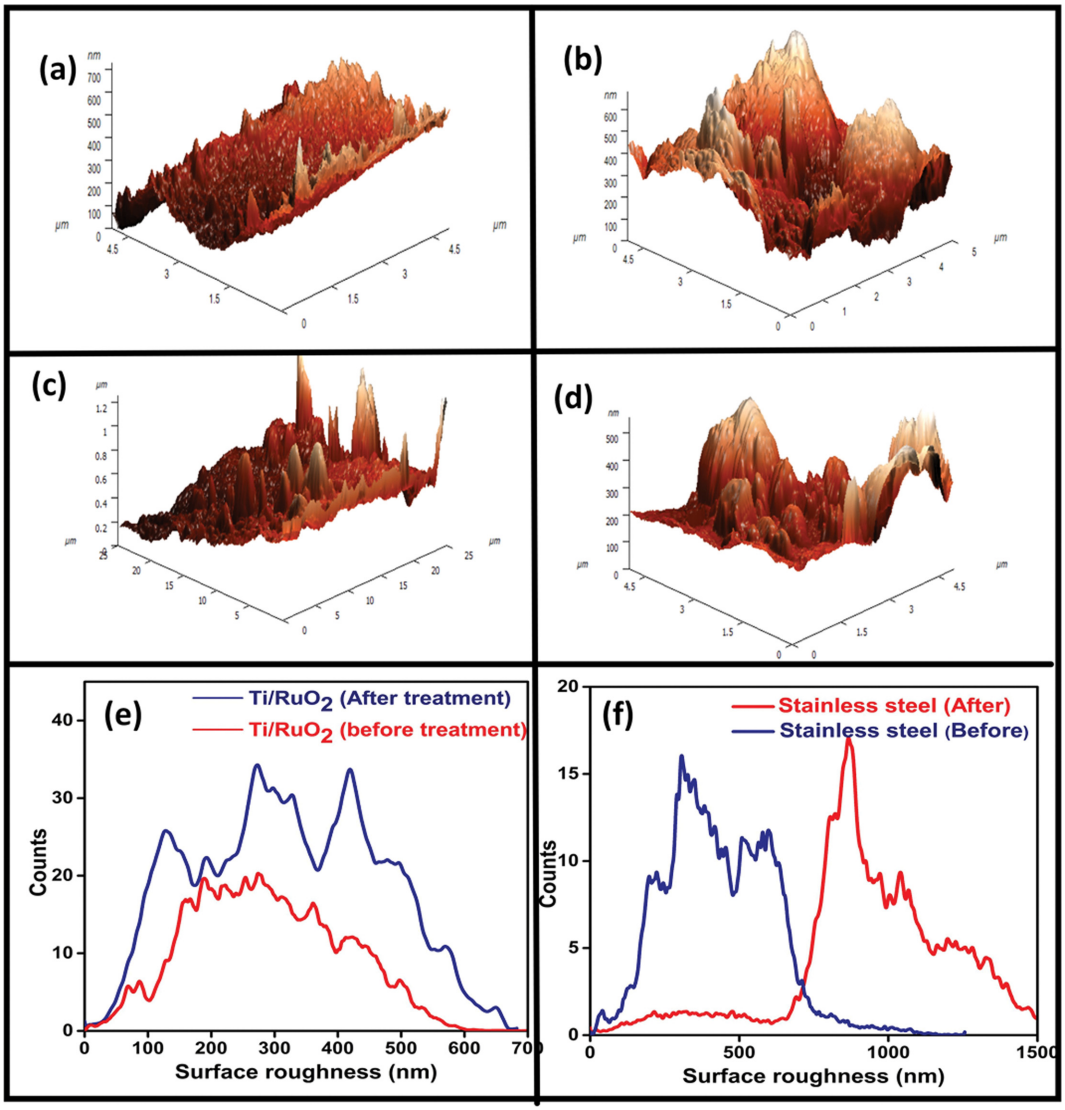


Fig. 5. 3-D images of (a) Ti/RuO_2 before treatment, (c) Ti/RuO_2 after treatment, (b) S.S before treatment, (d) S.S. after treatment process, (e) Histogram analysis for Ti/RuO_2 and (f) stainless steel.

regression model are calculated using the ANOVA tool as represented in Eqs. (13) and (14)

$$R^2 = 1 - \Sigma_{i=1}^{N} \frac{(y_{i,cal} - y_{i,exp})^2}{(\bar{y}_{exp} - y_{i,exp})^2} \quad (13)$$

$$R^2_{adj} = 1 - \left((1 - R^2)\frac{n-1}{n-k-1}\right) \quad (14)$$

where $y_{i,cab}$ $y_{i,exp}$ are the calculated and experimental values of response variables, respectively; n is the number of data points, and k is the magnitude of parameter studies.

For optimizing the design of experiments, Design-Expert 13 (Stat-Ease Inc., Minneapolis, USA) software was used by applying the CCD method. We considered initial pH, current, initial concentration, and time (A, B, C, and D, respectively) as independent variables, and degradation percentage, COD removal percentage, and energy consumption (Y_1, Y_2, and Y_3, respectively) as three response variables. Other parameters such as stirring speed and electrode distance were kept constant (300 rpm and 0.5 cm, respectively) during the whole process to study the responses of the more influential factors. Each independent variable (A, B, C, and D) factors have their low, medium, and high values, which is represented in the coded form as the levels −1, 0, and 1, respectively. The range of the input parameters was decided using a literature study. Table

Table 1. Independent variables with their corresponding levels

Independent variables	Codes	Units	Levels		
			−1	0	1
Initial pH	A	-	2	6	10
Current	B	A	0.5	1.25	2
Initial concentration	C	ppm	50	125	200
Time	D	Min	2	8.5	15

Table 2. Experimental designed matrix with measured and predicted responses (M: measured value, P: predicted value)

Run	Independent variables				% Dye degradation		% COD Removal		Energy consumption	
	Initial pH	Current (A)	I.C (ppm)	Time (min)	M	P	M	P	M	P
1	10	2	50	2	59.45	61.52	40.21	38.92	4.033	4.19
2	2	1.25	125	8.5	76.7	77.19	52.5	52.98	7.5	7.5
3	10	0.5	200	15	81.78	80.01	58.42	58.31	2.93	2.77
4	6	1.25	125	8.5	78.15	78.26	54.81	54.69	7.5	7.5
5	6	1.25	125	8.5	78.15	78.26	54.81	54.69	7.5	7.5
6	10	2	200	15	90.11	91.94	79.29	77.67	30.25	30.09
7	2	0.5	200	2	38.14	38.32	12.28	12.12	0.39	0.549
8	2	2	50	2	58.29	60.01	30.12	33.24	4.033	4.19
9	2	0.5	50	15	82.68	83.36	59.5	60.25	2.93	2.77
10	10	2	50	15	99.98	99.75	82.41	85.58	30.25	30.09
11	2	0.5	50	2	47.71	45.99	23.5	22.05	0.39	0.549
12	2	2	200	15	89.71	90.76	71.4	73.59	30.25	30.09
13	2	2	200	2	50.45	49.66	22.6	19.01	4.033	4.19
14	6	1.25	125	2	50.12	50.75	18.2	22.01	1.77	0.491
15	10	1.25	125	8.5	79.99	79.29	57.4	57.16	7.5	7.5
16	10	0.5	200	2	42.52	42.26	20.9	17.39	0.39	0.549
17	2	0.5	200	15	79.28	77.31	57.41	55.63	2.93	2.77
18	6	1.25	125	8.5	78.15	78.26	54.81	54.69	7.5	7.5
19	6	1.25	50	8.5	88.5	85.82	72.12	66.03	7.5	7.5
20	10	2	200	2	52.82	52.09	23.43	25.69	4.033	4.19
21	6	1.25	200	8.5	75.6	78.07	50.79	57.11	7.5	7.5
22	10	0.5	50	15	84.25	85.14	61.4	61.92	2.93	2.77
23	6	0.5	125	8.5	62.12	67.2	37.2	42.13	1.66	1.66
24	10	0.5	50	2	50.12	49.02	25.5	26.32	0.39	0.549
25	6	1.25	125	15	90.21	89.37	70.67	67.1	13.28	14.55
26	6	2	125	8.5	85.46	80.17	62.1	57.41	17.14	17.14
27	6	1.25	125	8.5	78.15	78.26	54.81	54.69	7.5	7.5
28	6	1.25	125	8.5	78.15	78.26	54.81	54.69	7.5	7.5
29	2	2	50	15	99.12	99.49	82.06	82.5	30.25	30.09
30	6	1.25	125	8.5	78.15	78.26	54.81	54.69	7.5	7.5

1 shows all the independent variables used with their corresponding levels by using CCD approach. Total 30 sets of experiments were conducted in random order containing 2^k=24=16 fractional points, 2k=2×4=8 axial points and 6 centre points where k=4 [50].

Table 2 displays the independent variable matrix of 30 sets of experiments designed by the RSM and the experimental values of the responses and the predicted values of the responses (calculated using Eqs. (15), (16), and (17)) of each set were compared. The characteristic of the wastewater from the dyeing unit before and after the treatment process is presented in Table S2.

7. Analysis of Variance (ANOVA) and Model Fitting

Dye degradation, COD removal, and energy consumption were calculated using the following quadratic equations of the empirical model developed for responses Y_1, Y_2, and Y_3 of input variables A, B, C, and D in coded form.

(a) Dye degradation

$$Y_1=78.26+1.05\times A+6.49\times B-3.87\times C+19.31\times D-0.3794\times A\times B+0.2281\times A\times C-0.3119\times A\times D-0.6694\times B\times C+0.5256\times B\times D+0.4056\times C\times D-0.0154\times A^2-4.57\times B^2+3.69\times C^2-8.20\times D^2 \quad (15)$$

(b) COD removal

$$Y_2=54.69+2.09\times A+7.64\times B-4.46\times C+22.55\times D+0.3519\times A\times B+0.2506\times A\times C-0.6494\times A\times D-1.07\times B\times C+2.77\times B\times D+1.33\times C\times D+0.3763\times A^2-4.92\times B^2+36.88\times C^2-10.14\times D^2 \quad (16)$$

(c) Energy consumption

$$Y_3=7.50+0.000\times A+7.74\times B+0.000\times C+7.03\times D+0.000\times A\times B+0.000\times A\times C+0.000\times A\times D+0.000\times B\times C+5.92\times B\times D+0.000\times C\times D+0.000\times A^2+1.89\times B^2-0.0068\times C^2+0.0182\times D^2 \quad (17)$$

After neglecting the insignificant terms (p values <0.05) shown in Table 3, Eqs. (15), (16), and (17) were modified to the reduced fitted model equations for dye degradation, COD removal, and energy consumption, respectively, as

$$Y_1=78.26+6.49\times B-3.87\times C+19.31\times D-0.6694\times B\times C+0.5256\times B\times D+0.4056\times C\times D-8.20\times D^2 \quad (18)$$

Table 3. ANNOVA output for regression model. 1: R^2=0.9889, Adjusted R^2=0.9785, Predicted R^2=0.9436; 2: R^2=0.9814, Adjusted R^2=0.9641, Predicted R^2=0.9027; 3: R^2=0.9986, Adjusted R^2=0.9972, predicted R^2=0.9938

Source	Sum of squares	Mean square	Degree of freedom(df)	F-value	P-value (Prob>F)	Significance
Model (dye degradation[1])	12,152.89	868.06	14	65.24	<0.0001	significant
A-Initial pH	453.11	453.11	1	30.05	0.0557	
B-Current	349.18	349.18	1	26.24	0.0001	
C-Initial concentration	300.70	300.70	1	22.60	0.0001	
D-Time	7,873.0	7,873.0	1	591.70	<0.0001	
AB	1.80	1.80	1	0.1349	0.7185	
AC	55.20	55.20	1	4.15	0.0597	
AD	72.34	72.34	1	0.44	0.0541	
BC	2.94	2.94	1	1.2210	0.0450	
BD	284.93	284.93	1	21.41	0.0003	
CD	134.33	134.33	1	10.10	0.0062	
A^2	34.49	34.49	1	2.59	0.1282	
B^2	0.1665	0.1665	1	0.0125	0.9124	
C^2	0.1600	0.1600	1	0.0120	0.9141	
D^2	655.71	655.71	1	49.28	<0.0001	
Residual	199.59	13.31	15			
Lack of fit	199.59	19.96	10			
Pure error	0.0000	0.0000	5			
Corr. total	12,352.48		29			
Model (COD removal[2])	20,047.76	1,431.9	14	45.26	<0.0001	significant
A-Initial pH	164.65	164.65	1	5.20	0.0518	
B-Current	417.99	417.99	1	13.21	0.0024	
C-Initial concentration	492.35	492.35	1	15.56	0.0013	
D-Time	13,125.78	13,125.7	1	414.89	<0.0001	
AB	29	29	1	0.9166	0.3535	
AC	53.36	53.36	1	1.69	0.2136	
AD	0.1406	0.1406	1	0.0044	0.9477	
BC	232.11	232.11	1	7.34	0.0162	
BD	287.81	287.81	1	9.1	0.0087	
CD	231.19	231.19	1	7.31	0.0164	
A^2	41.16	41.16	1	1.3	0.2719	
B^2	17.17	17.17	1	0.5426	0.4727	
C^2	14.97	14.97	1	0.4733	0.502	
D^2	1,881.92	1,881.92	1	59.48	<0.0001	
Residual	474.55	31.64	15			
Lack of fit	217.17	47.46	10			
Pure error	0.0000	0.0000	5			
Corr. total	20,522.32		29			

$$Y_2=54.69+7.64\times B-4.46\times C+22.55\times D-1.07\times B\times C+2.77\times B\times D+1.33\times C\times D-10.14\times D^2 \quad (19)$$

$$Y_3=7.50+7.74\times B+7.03\times D+5.92\times B\times D+1.89\times B^2 \quad (20)$$

The 'model F-value' was calculated by software as 95.28, 56.64, and 748.40 for dye degradation, COD removal, and energy consumption, respectively, depicting that model is significant. The chance that this large F-value could occur due to noise is only 0.01%. Similarly, 'Prob>F' values for these models were found to be less than 0.0001 (it should be less than 0.0500), which indicates that the models are significant. If the values are greater than 0.1000, model terms are not significant. Reduction of the model may be required if there are many insignificant terms.

There are several other terms, such as standard deviation (SD), coefficient of variation (CV), coefficient of determination (R^2), adjusted R^2 (R_{adj}), and predicted R^2 (R_{pred}), used to define the model accuracy. SD values for degradation, COD removal, and energy consumption should be small. These are given as 2.51, 3.81, and 0.493. Their corresponding CV values are 3.45, 7.61, and 5.71, respectively, showing the reliability of the experiments. For dye degrada-

Table 3. Continued

Source	Sum of squares	Mean square	Degree of freedom(df)	F-value	P-value (Prob>F)	Significance
Model (energy consumption^3)	2,554.57	182.47	14	748.40	<0.0001	significant
A-Initial pH	0.0000	0.0000	1	0.0000	1.0000	
B-Current	1,078.52	1,078.5	1	4,423.5	<0.0001	
C-Initial concentration	0.0000	0.0000	1	0.0000	1.0000	
D-Time	889.55	889.55	1	3,648.5	<0.0001	
AB	0	0	1	0	1	
AC	0	0	1	0	1	
AD	0	0	1	0	1	
BC	0	0	1	0	1	
BD	560.6	560.6	1	2,299.3	<0.0001	
CD	0	0	1	0	1	
A^2	0.0001	0.0001	1	0.0005	0.9826	
B^2	9.29	9.29	1	38.09	<0.0001	
C^2	0.0001	0.0001	1	0.0005	0.9826	
D^2	0.0009	0.0009	1	0.0035	0.9535	
Residual	3.66	0.2438	15			
Lack of fit	3.66	0.3657	10			
Pure error	0.0000	0.0000	5			
Corr. total	2,558.23		29			

tion, R_{pred}=0.9436 and R_{adj}=0.9785; for COD removal, R_{pred}=0.9027 and R_{adj}=0.9641; for energy consumption, R_{pred}=0.9938 and R_{adj}= 0.9972. These R_{pred} and R_{adj} are in reasonable agreement as their difference is less than 0.2. The R^2 value of these models is 0.9889, 0.9814, and 0.9986 for degradation, COD, and energy consumption, i.e., near to unity, which implies the models gave accurate responses. The straight-line plots between the actual values (measured response) and the predicted values (approximate function value) show that experimental data and the predicted data are nearly the same (Fig. S3). The plot between the normal % probability and externally studentized residual is a straight line that depicts data is normally distributed (Fig. S3).

8. Plackett-Burman Design for Selecting Significant Factors

Plackett-Burman design has been used for screening the variables and selecting the significant factors in Design-Expert software [51]; 43 factorial design has been selected and four independent variables were used (pH, current, initial concentration, and time) for the screening test. The remaining factors were renamed as dummy variables that are placeholders for designing the experiment. The level of significance of the factors can be seen in the half-normal plots and the Pareto chart as depicted in Fig. 8. D is the most important factor and A is the least significant factor. Time, current, and initial concentration are the significant factors, whereas pH is not significant, which can also be proved by the p-value from the Table 3.

9. 3-D Surface Plots and Perturbation Curves

3-D surface plots are the interaction graphs between all independent variables (pH, time, initial concentration, and current) and the three responses with all possible significant interactive arrangements of these factors shown in Figs. 9 and 10 that are based on the regression Eqs. (18), (19), (20); perturbation plots are used for comparison of all independent factors at a specific point in design space. Design-Expert software, by default, builds one reference point at the midpoint (coded value 0). The responses of these independent factors are plotted by changing only one factor and keeping other factors constant over the particular range. More steep is the plot factors with more sensitivity toward the response. Less steep is the plot factors that may be insensitive or less sensitive toward the response (Fig. S4). These curves may help determine the influential factors among all the factors for a particular response [52].

10. Extrapolation of the Significant Variables

For extrapolation of the important variables, the range of the time, current and initial concentration was increased from (2-15 min) to

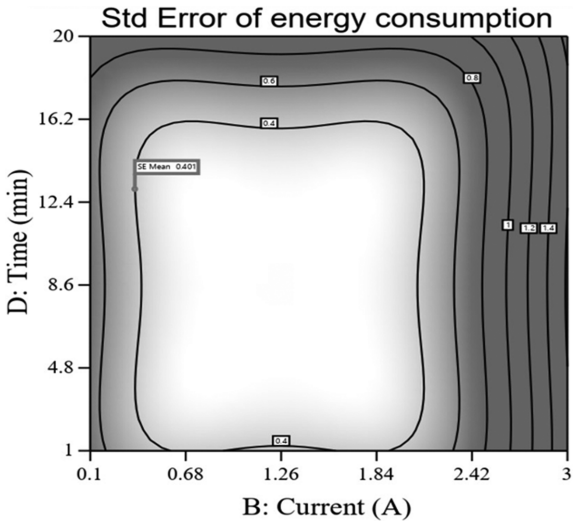


Fig. 6. Standard error contour of energy consumption for current and time.

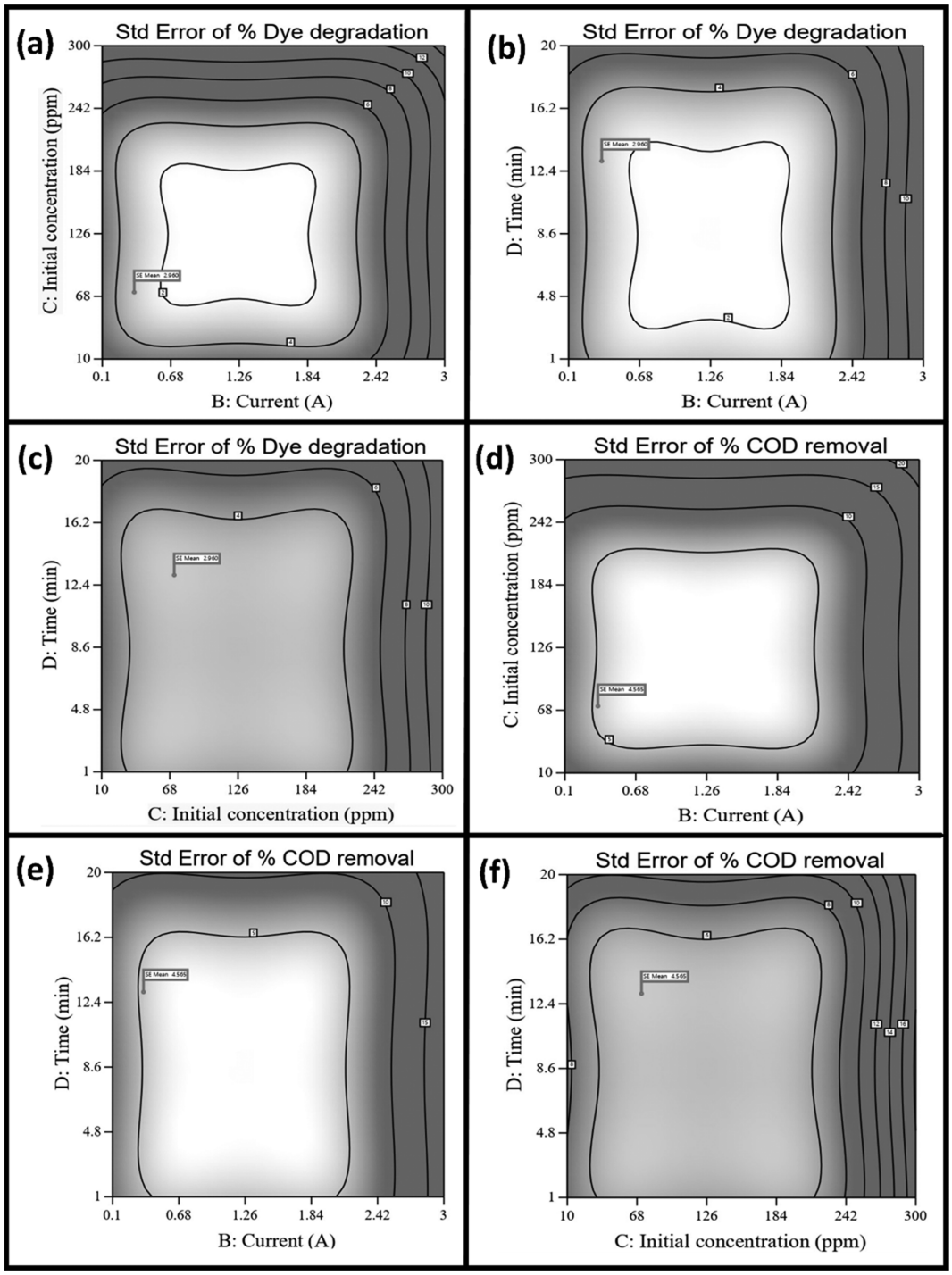


Fig. 7. Standard error contours of dye degradation (a), (b), (c) and COD removal (d), (e), (f).

(1-20 min), (0.5-2 A) to (0.1-3 A) and (50-200 mgL^{-1}) to (10-300 mgL^{-1}) and standard error was calculated by the Design-Expert software. The contours of the standard error for dye degradation percentage, COD removal, and energy consumption of significant interaction factors are shown in Fig. 6 and 7. The extrapolated area of the contours of the expanded axes is shaded. The specified factorial range area is lighter than the expanded area, which is darker. The standard errors for the responses of the extrapolated variables are 2.96, 4.56, and 0.40 for dye degradation, COD removal, and energy consumption, respectively.

11. Effects of Parameters (pH, Time, Current, Initial Concentration) on Responses

11-1. Dye Degradation and COD Removal

The pH of the solution varies from acidic to neutral to basic (2-10). pH has not significantly impacted on the degradation rate and COD. With changing the pH from acidic to basic, degradation does

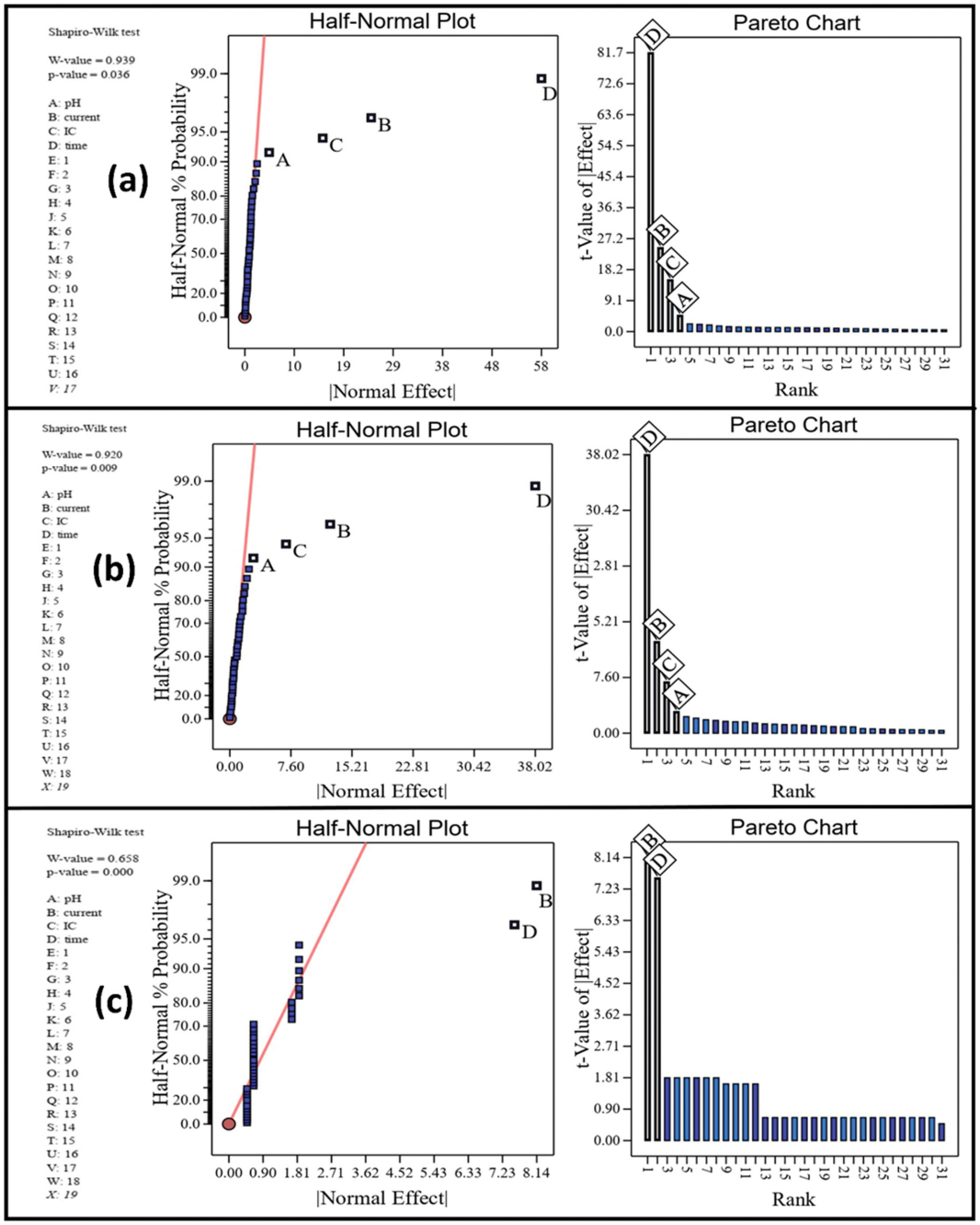


Fig. 8. Half normal and Pareto chart for (a) dye degradation (b) COD removal, and (c) energy consumption.

not get a significant influence. It can also be seen from the perturbation curve (A curve in supplementary Fig. S4(a) and (b)) that deviation is very less for pH. The dye degradation percentage and COD removal values at pH 2 were 65.25 and 20.51, respectively, at current 0.5 A, initial concentration 50 mg/L, and time 2 min. At pH 10, dye degradation and COD removal were 40.22% and 15.25% at the same response parametric values, respectively. According to the ANOVA result (Table 3), its p-value is 0.0557 for dye degradation, greater than 0.05, showing its insignificance, and the p-value is 0.0518 for COD removal. As the pH increases, hydroxyl ion production also increases. More hydroxyl ions can participate in the reaction to adsorb the dye [53]. In an acidic medium, OH^- ions are unstable, and in a basic medium, OCl^- are readily formed, contributing to a faster reaction rate [54]. More experiments were conducted in the pH range (2-10) and keeping current 2 A, initial concentration of 50 mg/L, and NaCl concentration 0.2 M for dye degradation and COD removal percentages. Similar trends were found as dye degradation, and COD removal increased significantly less, as represented in the supplementary Fig. S5(c). Chatzisymeon et al. [55] also reported that the pH of the solution for textile effluent does not affect the color removal for a 10-15 min reaction.

The current has a significant effect on both dye degradation and

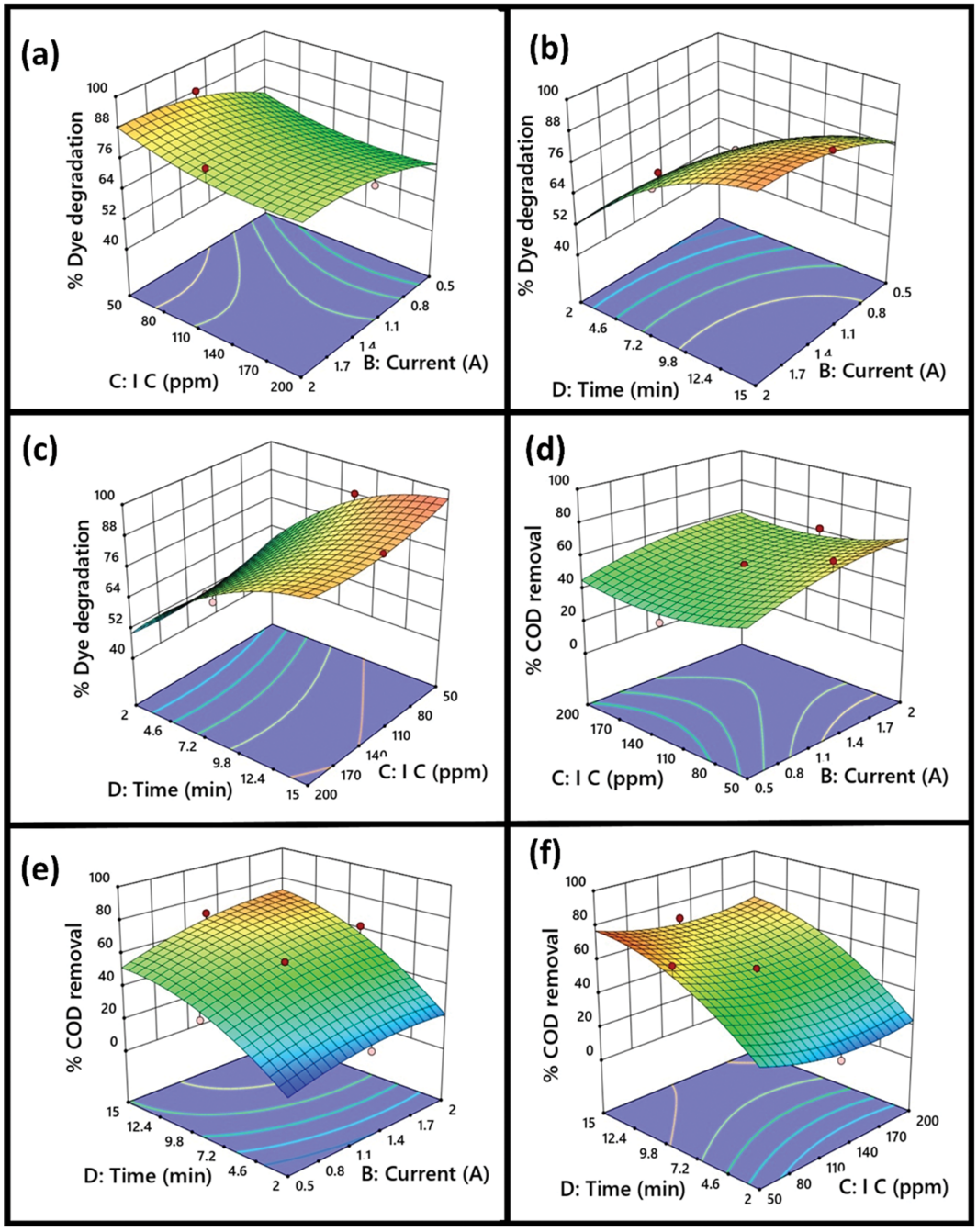


Fig. 9. 3-D plots for dye degradation with, (a) initial concentration and current, (b) time and initial concentration, (c) time and current and COD removal with (d) initial concentration and current, (e) time and current, (f) time and initial concentration.

COD removal, as shown in ANOVA Table 3. The current applied (0.5 A-2 A) is the most influential factor, as shown in supplementary Fig. S4(a) and (b) curve b, where the perturbation curve shows steep deviation. With a small increase in current density, both degradation rate and COD removal increase sharply, as shown in the 3-D surface graph (Fig. 9). The dye degradation and COD removal value at current 0.5 A was 38.22% and 12.0%, respectively, at pH, initial concentration, and time of 2, 200 mg/L, and 2 min, respectively. Their value at the same operating conditions for current 2 A is 60.12% and 15.13%. Its p-value from ANOVA Table 3 for the dye degradation and COD removal is less than 0.0001, which shows that it has significant terms for both responses. As the current increases, more oxidants such as chlorine/hypochlorite increases are produced that increases the reaction rate [56-58]. As depicted in supplementary, Fig. S5(a) also agrees with the increasing trend of the dye degradation and COD removal with increasing current from 0.5 A to 2 A at pH 7, initial concentration 50 mg/L, and 0.2 M NaCl. At the current of 0.5 A, the dye degradation and COD removal were 96.1% and 81%, respectively, in 15 min. At 2 A, current dye degradation and COD removal were 99% and 88%, respectively.

Körbahti et al. [59] reported the importance of current density in dye degradation. They varied the current density from 0.8 to 4.0 mA/cm^2 with 86.7% decolorization for 0.8 mA/cm^2 and 96.6% decolorization for 4 mA/cm^2 for AB29 dye. Khan et al. [60] reported that degradation of the NB dye changes from 20% to 100% when the current density changes from 8 mA/cm^2 to 20 mA/cm^2 at 0.056 M Na_2SO_4. Feng et al. [61] also reported the same trend and showed the effect on RB5 removal at different current, with the removal of 91.6% dye at 0.4 A in 50 min and 72.3% at 0.2 A.

The initial concentration of the dye (50 mg/L-200 mg/L) and electrolysis time (2-15 min) are essential factors for finding the reaction rate. More initial concentration means more dye molecules are present for the same number of oxidants if all other factors are kept constant, which lowers the rate of decoloration [62]. At the lowest initial concentration of 50 mg/L, the dye degradation and COD removal are 95.44% and 72.26%, respectively, keeping the pH values, current, and time as 10, 0.5 A, and 15 min, respectively. Its p-value is 0.0001, and 0.0002 for dye degradation and COD removal from Table 3 shows its significance. Reaction time is the most influential factor for decoloration efficiency. As the time increases, the efficiency of the reaction increases faster as shown in supplementary Fig. S5(d) and Fig. S4(a) and (b). Kaur et al. [63] show the gradual depletion of the AB and BB dye at 2 g/L NaCl, 100 mg/L initial dye concentration at 25 °C temperature, 30 mA/cm^2 current density, and 3 pH. Fig. 9 also shows the dependence of the dye degradation on the initial concentration of the dye. A similar trend of decreasing degradation with increasing dye concentration (50-200 mg/L) was obtained. 99% dye was degraded at initial concentration 50 mg/L, pH 7, current 2 A, and 0.2 M NaCl in 15 min, and 94% dye was degraded at the same operating conditions. Elbatea et al. [64] reported dye removal of 94.5% and COD removal of 79% for 50 mg/L Red 195 dye and dye degradation of 86.7% for 200 mg/L dye in 1 h.

11-2. Energy Consumption

Energy consumption evaluation is an important part of the whole electrochemical process as the process should be energy efficient. Energy consumption is calculated from Eq. (17). The interactive effect of significant parameters is shown in Fig. 10. pH and initial concentration are insignificant terms as their p-value is 1.000, greater than 0.050. From perturbation curves (Fig. S4(c)) also, we can see that there is no deviation in the curves of both factors. Fig. 10 confirms that energy consumption increases with an increase in current value (0.5 A-2 A) for all values of pH and initial concentration

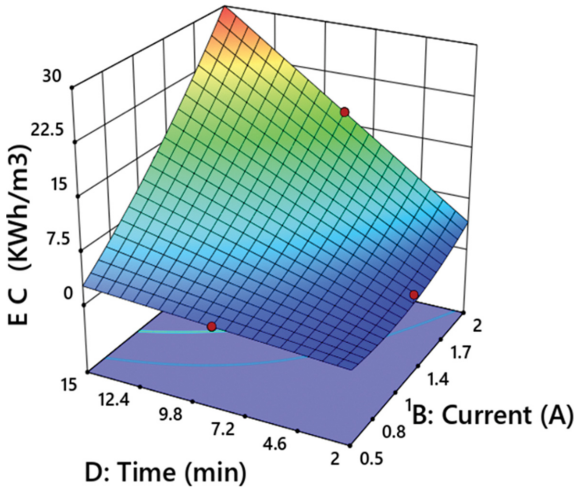


Fig. 10. 3-D plots for energy consumption with, (a) time and current.

at 6 pH and 8.5 min time. Current is considered the most important factor affecting energy consumption as its p-value is also less than 0.001 from ANOVA Table 3. Minimum energy consumption is 0.39 KWh/m^3 at pH 10, current 0.5 A, initial concentration 200 mg/L, and time 2 min. Maximum energy consumption is 30.25 KWh/m^3 at pH 2, initial concentration 200 mg/L, and time 15 min. Perturbation curve B also shows more deviation from the reference point (Fig. S4(c)). This is because with the rise in current, potential difference increases, which causes an increase in energy consumption. The electro-oxidation process accelerates with its increase and reduces reaction time, but also electrode consumption becomes faster [65-67]. The supplementary Fig. S5 also depicts the increase in the energy consumption with the change in the current from 0.5 A to 2 A. Kuleyin et al. [68] reports an increase in energy consumption from 9.1 KWh/m^3 to 27 KWh/m^3 for a current value of 0.35 A and 0.75 A in 60 min in batch electro-Fenton system for real textile wastewater. Hussain et al. [69] found the maximum removal (99.2%) of food dye for 0.340 KWh/m^3 of energy consumption at 2.70 mA/cm^2, 4.15 pH, 0.065 M NaCl concentration and minimum removal of 1.420% at 0.917 KWh/m^3.

Increasing the reaction time from 2 min to 15 min, energy consumption increases at 6 pH and 1.25 A current. From the ANOVA Table 4, we can also see that its p-value is less than 0.001, i.e., it is a significant term for the response. The steep curve in the perturbation

Table 4. Some of the advanced oxidation processes used in the wastewater treatment

Process	Adsorbent/Catalyst	Dye	Comments	Ref.
Photo-Fenton	Amino-Fe_3O_4-functionalized graphene oxide	RB5	Color removal-75%	[72]
Adsorption	Amino graphene oxide	MB	maximum adsorption capacity-53 mg g^{-1}	[73]
Adsorption	Polystyrene fibers with graphene oxide	MB	Color removal-100%	[74]
Photo-Fenton	Multilayer graphene oxide	textile wastewater	Organic matter removal-76.36%	[75]
Ozonation	-	Rezomal Black B	Color-%	[76]
Electro-oxidation	Ti/RuO_2 anode	RB	Color removal-99.12% COD removal-82.6%	

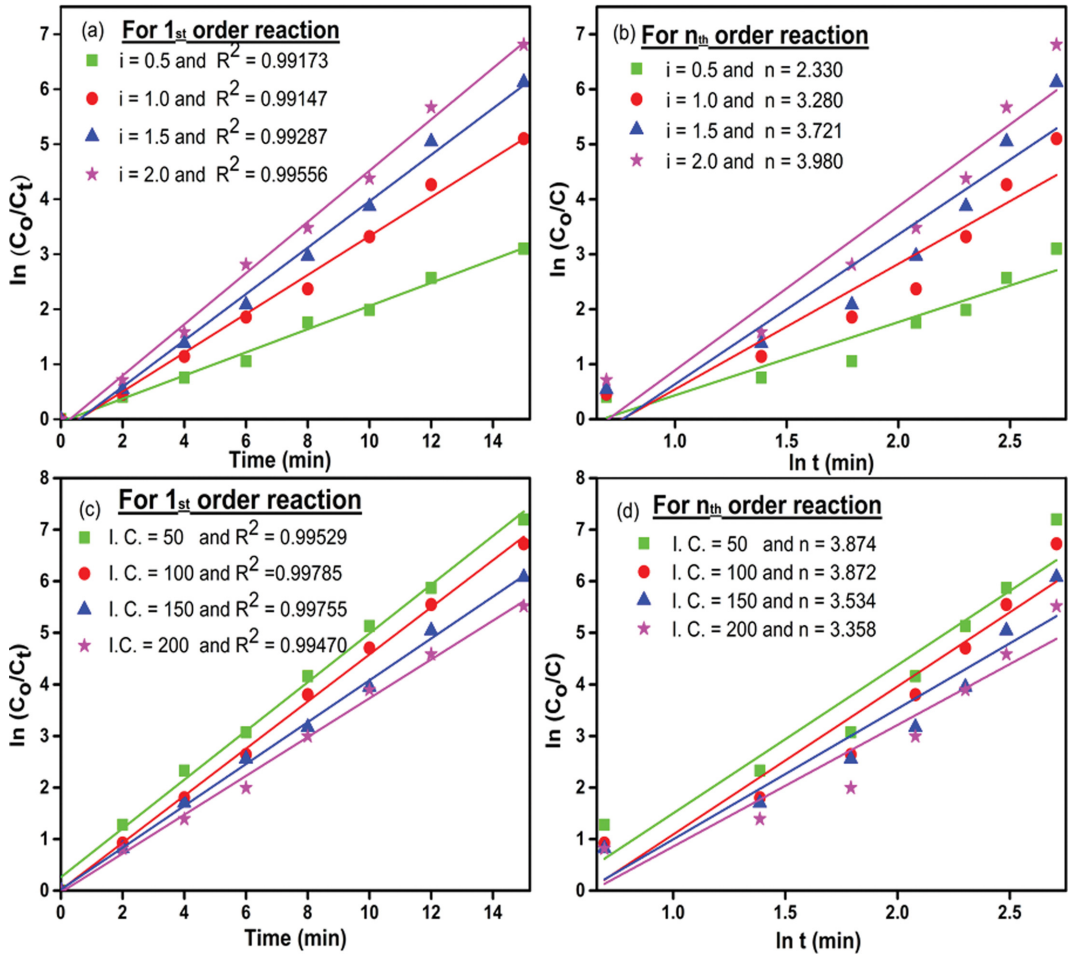


Fig. 11. Kinetics of the (a) 1st order reaction for different current values, (b) nth order reaction at different current values, (c) 1st order reaction at different initial concentration, (d) nth order reaction at different initial concentration.

curve also shows its influence on the response energy consumption.

Optimized values obtained to maximize the dye degradation and COD removal and minimize the energy consumption are at initial pH 3.3, current 0.5 A, time 9.4 min for dye degradation of 99.82%, COD removal of 82.50%, and energy consumption of 1.817 KWh/m^3 with desirability 1. These optimized values were validated by conducting three sets of experiments at the same optimized condition. The values of dye degradation, COD removal, and energy consumption were 99.01%, 82.22%, and 1.95 KWh/m^3, respectively. This shows that the optimized values obtained by the theoretical model are in agreement with the experimental values. This ensures the accuracy and good precision of the model surface model. A comparative assessment of some advanced oxidation processes used for textile wastewater treatment is summarized in Table 4. But there are some disadvantages of the mentioned methods. The drawbacks of the ozonation process, according to the US EPA 1999, include less reduction of COD and BOD values of wastewater, the requirement of complex equipment and control systems, and the operating and maintenance cost requirements are also high [70]. The shortcomings of the Fenton and photo Fenton process include too low pH required in the process, a high concentration of chemical reagents being required, and a high amount of iron sludge is also produced [71]. Therefore, the electrochemical process is used in this paper, which is also described in the introduction section.

12. Degradation Kinetic Study

A kinetic study was done by plotting the graph between concentration and time using Eqs. (5) and (8), and average relative error was calculated using Eq. (10). The best model could be found if the plotted graph is fitted according to the model equation with minimum permissible error. Here 1st order is the best fitted model with all R^2 values greater than 0.9 for all i (A) (0.5, 1.0, 1.5, 2.0) and I.C (mg/L) (50, 100, 150, 200). Graphs for kinetic study of 1st and nth order are shown in Fig. 11 at different i (A) and different I.C (mg/L). Rate constant was calculated from the slope of Eq. (5) for 1st order and rate constant and the order of the reaction from Eq. (9) for nth order reaction as shown in Table 5. For the 1st order model reaction, it was found that the rate constant increases with the increase of the current, and with increasing, the initial concentration rate constant decreases with the relative error in an acceptable limit. For 1st order reaction, the maximum value of k is 0.473 with an R^2 value of 0.996 at 50 ppm I.C, and at i=2, A maximum value of k is 0.466 with R^2=0.996. There is no particular trend for the nth order reaction. Maximum value of k=2.166 of order n= 3.280 and R^2=0.879 at i (A)=1.0. The maximum value at I.C=200

Table 5. Kinetics for 1st order and nth order reaction at varied current and initial concentrations

i (A)	Order of the reaction (n)	Rate constant (k)	R^2	% Relative error
For 1st order reaction				
0.5	1	0.211	0.992	0.058
1.0	1	0.353	0.991	0.168
1.5	1	0.422	0.993	0.199
2.0	1	0.466	0.996	0.151
For nth order reaction				
0.5	2.330	1.95	0.876	0.596
1.0	3.280	2.166	0.879	1.689
1.5	3.721	2.150	0.877	2.458
2.0	3.980	2.015	0.902	2.317
I.C (ppm)	Order of the reaction (n)	Rate constant (k)	R^2	% Relative error
For 1st order reaction				
50	1	0.473	0.996	0.165
100	1	0.457	0.998	0.070
150	1	0.406	0.998	0.063
200	1	0.377	0.995	0.118
For nth order reaction				
50	3.874	1.61	0.914	1.859
100	3.872	1.860	0.910	1.928
150	3.534	1.835	0.899	1.722
200	3.358	1.891	0.883	1.759

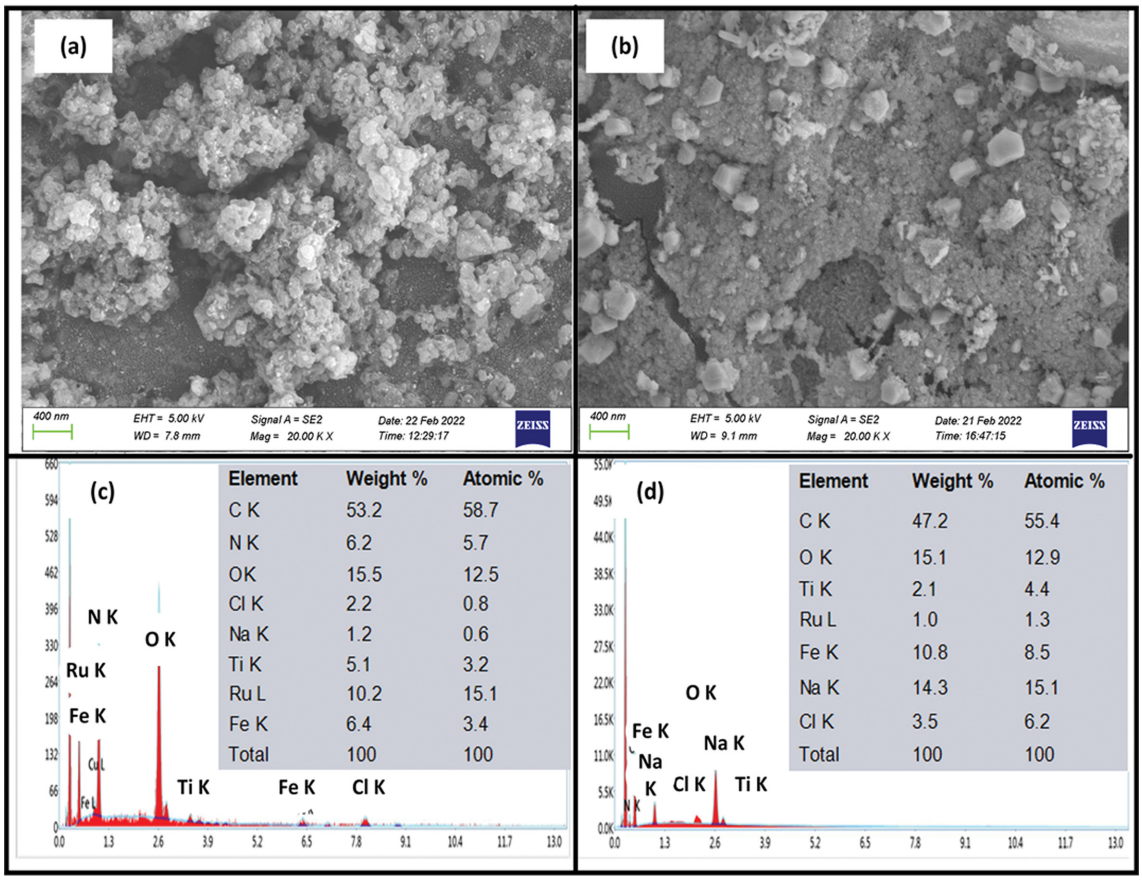


Fig. 12. FE-SEM images of sludge (a) 90 °C, (b) calcined at 600 °C, (c) EDX of sludge at 90 °C, (d) EDX of sludge calcined at 600 °C.

of k is 1.891 with R^2=0.883, and the order of the reaction is 3.358. The reaction is faster if the rate constant is more [77-80].

13. Sludge Characteristics

Sludge is produced when highly concentrated dye wastewater is treated with the electrochemical method. It is the chief problem in the textile wastewater treatment plant by electrochemical method on a large scale. Sludge can be treated, disposed of, or reused according to its composition. Therefore, characterization of the sludge is a vital part of knowing its composition [81-83]. A small amount of sludge is produced in the process described. It was first dried in the oven at 90 °C for 30 min and then calcined for 1 h at 600 °C [83]. SEM and EDX of the sludge are shown in Fig. 12. SEM images show the morphology of the clusters at 90 °C and 600 °C. Fig. 9(a) shows the spherical aggregates, and Fig. 12(b) shows the small rock-like structure, whereas EDX shows the presence of C, N, O, Cl, Ti, Ru, Fe, and Na elements and their composition in Fig. 12((c) and (d)). XRD images (Fig. S4(d)) also confirm the elements shown by EDX analysis with their corresponding planes (Fig. 12(c) and (d)). At 90 °C, the intensity of the peaks is very low, whereas at 600 °C intensities are high, which shows that the crystalline nature of the sludge increases after the calcination at 600 °C. The presence of C, N, and Cl shows that Rhodamine B gets absorbed at Ti and Ru. The presence of Na and Cl shows the electrolyte elements used for dissociation. Ti and Ru present in the sludge can be reused to treat textile

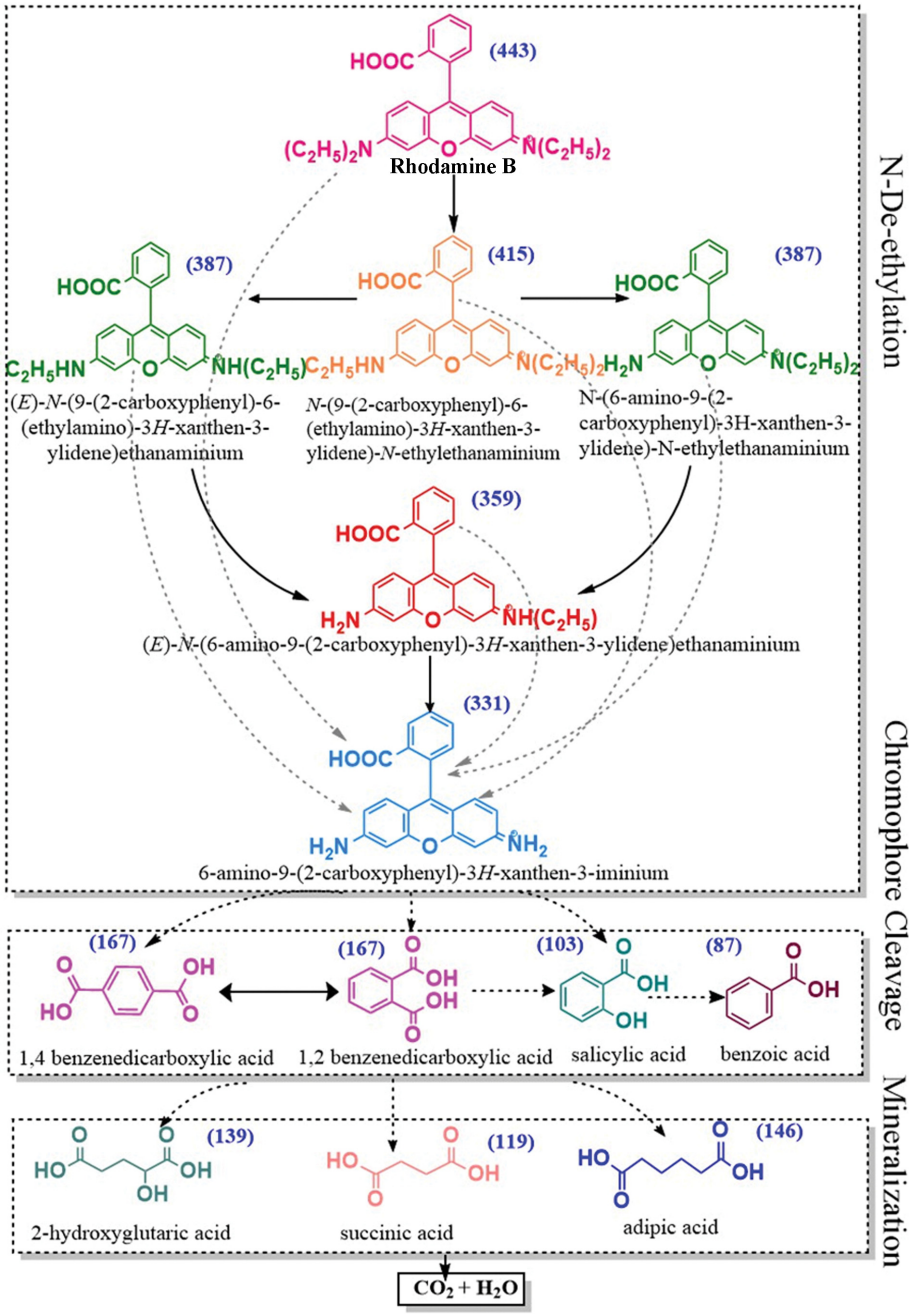


Fig. 13. Reaction mechanism of Rhodamine B dye degradation by Ti/RuO_2 anode.

Table 6. Total cost analysis of the treatment process including cost of fabrication and running cost of the process

Chemical/Material	Used quantity	Cost per measurement	Cost of used material
Cost of anode fabrication			
Ruthenium chloride	0.518 g	240₹/g	124.32₹
Ethylene glycol	2.144 ml	0.8₹/ml	1.795₹
Citric acid	1.4601	0.7₹/g	1.022₹
Titanium sheet	22 cm^2	16.66₹/cm^2	366.52₹
Stainless steel sheet	22 cm^2	0.416₹/cm^2	9.166₹
Energy consumption	14 kWh	5.65₹/kWh	79.1₹
Total Cost$_{anode}$			581.59₹ or 7.66$
Running cost of the electrochemical process			
NaCl	2.366 g	0.6₹/g	1.2₹
Energy consumption	1.817 KWh/m^3	5.65₹/KWh	0.002₹
Total Cost$_{running}$			1.202₹ or 0.016$
Total cost of the process=Cost$_{anode}$+Cost$_{running}$			582.79₹ or 7.68$

wastewater. Further work has been carried out in our lab to study the sludge's reusability.

14. Reaction Mechanism

Redox reaction happens in the above process to give CO_2 and H_2O the final product. Hydroxyl ion (OH^-) is formed at the surface of the cathode by breaking the H_2O molecule, and metal oxide (RuO_2) from the anode reacts with OH^- to form metal hydroxide ($MO_x(OH^-)$) as shown in Eq. (18). Active anodes such as Ti/RuO_2 can degrade the organics by direct or indirect oxidation. It will depend on the solution pH and concentration of chloride ions [50, 84]. In an acidic pH solution, more oxidants like Cl_2, ClO^- and HOCl are produced for indirect oxidation. At basic pH, due to the high reactivity and instability of the OH^-, more H_2O_2 and HO_2^- will get produced as shown in Eqs. (18), (19), (20) for direct oxidation. In direct oxidation following reaction will take place:

$$MO_x+H_2O\rightarrow MO_x(\cdot OH)+H^++e^- \quad (18)$$

$$R+MO_{x+1}\rightarrow RO+MO_x \quad (19)$$

$$R+MO_x(\cdot OH)\rightarrow CO_2+H^++e^-+MO_x \quad (20)$$

If the chlorides are present in the solution, ClO^- and $HOCl^-$ oxidants are formed shown in reactions (21), (22), (23) for indirect oxidation:

$$2Cl^-\rightarrow Cl_2+2e^- \quad (21)$$

$$Cl_2+H_2O\rightarrow HOCl+H^++Cl^- \quad (22)$$

$$HOCl+OH^-\rightarrow ClO^-+H_2O \quad (23)$$

All intermediates were found by UPLC-QTOF/MS, and the spectrums are shown in the supplementary Table S3. Degradation of rhodamine B dye takes place in three major steps: (1) N-de-ethylation, (ii) chromophore cleavage, and (iii) mineralization. First step includes breaking of N-ethyl group present on the Rhodamine B dye structure by OH^- to form the intermediates*(E)-N*-(9-(2-carboxyphenyl)-6-(ethylamino)-3*H*-xanthen-3-ylidene)-*N*-ethylethanaminium (*m/z*=415),*(E)-N*-(9-(2-carboxyphenyl)-6-(ethylamino)-3*H*-xanthen-3-ylidene)ethanaminium (*m/z*=387), *N*-(6-amino-9-(2-carboxyphenyl)-3*H*-xanthen-3-ylidene)-*N*-ethanaminium (*m/z*=387), *(E)-N*-(6-amino-9-(2-carboxyphenyl)-3*H*-xanthen-3-ylidene) ethanaminium (*m/z*=359), 6-amino-9-(2-carboxyphenyl)-3*H*-xanthen-3-iminium (*m/z*=331). The second step involves the cleavage of the conjugated chromophore structure into aliphatic chains responsible for the decolorization of the dye. Possible intermediates formed were 1,4 benzenedicarboxylic acid (*m/z*=167), 1,2 benzenedicarboxylic acid (*m/z*=167), salicylic acid (*m/z*=103), benzoic acid (*m/z*=87). The chromatographs of the intermediates with their m/z, intensities and retention time are given in supplementary data (Table S3). However, hydroxyl radicals could directly attack the center of the benzene ring to form aliphatic compounds. The last step is mineralizing the smaller molecular weight compounds into CO_2 and H_2O [85,86]. The full mechanism is pictured in Fig. 13.

15. Cost Analysis

The total cost of the process (Cost$_{process}$) was calculated with the help of calculating the cost of the anode fabrication (Cost$_{anode}$) and the running cost of the process (Cost$_{running}$). The total cost of the process (Cost$_{process}$)=the cost of the anode (Cost$_{anode}$)+the cost of running the process Cost$_{running}$. The cost of the anode includes all the cost of the materials or chemicals used shown in Table 6. In India, the electricity price is 5.65₹/kWh [87]. Energy consumption for 7 h usage of the 2,000 W equipment is 14 kWh, which costs ₹79.1. Therefore, the total cost of the fabrication is ₹581.59, or $7.66. Running cost is also shown in Table 6. Energy consumption at the optimized values of the parameters by RSM (pH 3.37, current 0.5 A, initial concentration 50 mg/L, time 9.4 min) is 1.817 kWh/m^3 for 99.822% dye degradation 82.50% COD removal. The value of energy consumption comes out to be 10.26₹/m^3. For 200 mL of wastewater, it is ₹0.016 or $0.0002053. For 1 L of the wastewater, it will become ₹0.0102. Therefore, the total cost of the process is ₹582.79 or $7.68. However, this calculation is for batch scale; for large scale processes, the cost of anode fabrication will decrease the cost-effectiveness.

CONCLUSION

This study notes the textile wastewater dye degradation, COD removal, and energy consumption of the treatment process. 0.2 M NaCl was used as an electrolyte which was kept constant during

the whole process. Ti/RuO_2 anode was fabricated using the sol-gel method. Characterization of both the anode and cathode (stainless steel) was done before and after the experiments. Elemental composition and morphological structure were shown by FE-SEM and EDX. XRD also confirms the elements present and the phases of the elements. AFM shows surface roughness to be 96.9 nm and 119.421 nm before and after treatment, respectively, for the anode and 85.34 nm and 145.76 nm before and after treatment, respectively, for the cathode (increases for both the electrodes). pH has very less impact on dye degradation percentage and COD removal percentage, whereas current, initial concentration, and time have a significant effect on them. At current=2 A, initial concentration= 50 mg/L, time=15 min, and pH=2, the dye degradation is 99.12% and COD removal is 82.06%. Optimized values obtained to maximize the dye degradation and COD removal, and to minimize the energy consumption are at initial pH=3.3, current=0.5 A, initial concentration=50 mg/L, time=9.4 min for 99.82% dye degradation, 82.50% COD removal, and 1.817 kWh/m^3 with desirability 1. For first-order reaction, maximum value of k is 0.473 with R^2 value of 0.996 at 50 ppm I.C, and at i=2 A maximum value of k is 0.465 with R^2=0.996. Mechanism of the reaction has been found and reported, which agrees with the literature. The m/z ratios of the intermediates were found to be gradually decreased from 443 to 87, and finally, CO_2 and H_2O were formed. Sludge characteristics show its composition that can further be studied for its reusability. The total cost for 200 mL of wastewater is ₹582.79 or $7.68, including the cost of anode fabrication and the running cost of the process. For large-scale processes, cost-effectiveness will be less.

Funding

This research did not receive any specific grant from funding agencies in the public, commercial, or not-for-profit sectors.

Declaration of Competing Interest

The authors declare that they have no known competing financial interests or personal relationships that could have appeared to influence the work reported in this paper.

SUPPORTING INFORMATION

Additional information as noted in the text. This information is available via the Internet at http://www.springer.com/chemistry/journal/11814.

REFERENCES

1. D. A. Yaseen and M. Scholz, *Int. J. Environ. Sci. Technol.*, **16**, 1193 (2019).
2. T. Jiao, H. Zhao, J. Zhou, Q. Zhang, X. Luo, J. Hu, Q. Peng and X. Yan, *ACS Sust. Chem. Eng.*, **12**, 3 (2015).
3. J. Ma, M. Zhang, M. Ji, L. Zhang, Z. Qin, Y. Zhang, L. Gao and T. Jiao, *Int. J. Biol. Macromol.*, **193**, 2221 (2021).
4. J. Yin, F. Zhan, T. Jiao, H. Deng, G. Zou, Z. Bai, Q. Zhang and Q. Peng, *Chin. Chem. Lett.*, **31**, 4 (2020).
5. A. G. Vlyssides, D. Papaioannou, M. Loizidoy, P. K. Karlis and A. A. Zorpas, *Waste Manage.*, **20**, 7 (2000).
6. J. Iniesta, E. Exposito, J. Gonzalez-Garcıa, V. Montiel and A. Aldaz, *J. Electrochem. Soc.*, **149**, 5 (2002).
7. C. Barrera-Diaz, G. Roa-Morales, L. Avila-Cordoba, T. Pavon-Silva and B. Bilyeu, *Ind. Eng. Chem. Res.*, **45**, 34 (2006).
8. C. R. Costa, C. M. R. Botta, E. L. G. Espindola and P. Olivi, *J. Hazard. Mater.*, **153**, 616 (2008).
9. D. Xu, Y. Li, L. Yin, Y. Ji, J. Niu and Y. Yu, *Front. Environ. Sci. Eng.*, **12**, 1 (2018).
10. L. Zhang, K. Wei, J. Ma, J. Wang, Z. Liu, R. Xing and T. Jiao, *Appl. Surf. Sci.*, **566**, 150754 (2021).
11. S. Zhu, L. Fan and Y. Lu, *RSC Adv.*, **7**, 59939 (2017).
12. C. K. Caraújo, G. R. Oliveira, N. S. Fernandes, C. L. P. S. Zanta, S. S. L. Castro, D. R. da Silva and C. A. Martínez-Huitle, *Environ. Sci. Pollut. Res.*, **21**, 16 (2014).
13. N. Jiang, Q. Zhao, Y. Xue, W. Xu and Z. Ye, *J. Clean. Prod.*, **188**, 732 (2018).
14. A. M. S. Polcaro, S. Palmas, F. Renoldi and M. Mascia, *J. Appl. Electrochem.*, **29**, 2 (1999).
15. L. Zhang, L. Xu, J. He and J. Zhang, *Electrochim. Acta*, **117**, 192 (2014).
16. M. Ghazouani, L. Bousselmi and H. Akrout, *J. Environ. Chem. Eng.*, **8**, 104509 (2020).
17. A. J. Terezo and E. CPereira, *Mater. Lett.*, **53** 339 (2002).
18. A. Majedi, A. Abbasi and F. Davar, *J. Sol Gel Sci. Technol.*, **77**, 543 (2016).
19. S. Varala, V. Ravisankar, M. Al-Ali, M. I. Pownceby, R. Parthasarathy and S. K. Bhargava, *Chemosphere*, **237**, 124488 (2019).
20. K. Y. Nandiwale and V. V. Bokade, *Ind. Eng. Chem. Res.*, **53**, 18690 (2014).
21. E. Raissi and R. E. Farsani, *World Acad. Sci., Eng. Technol.*, **39**, 280 (2009).
22. K. Y. Nandiwale, A. M. Pande and V. V. Bokade, *RSC Adv.*, **5**, 22 (2015).
23. M. Abdulgader, Q. JimmyYu, A. A. Zinatizadeh, P. Williams and Z. Rahimi, *J. Environ. Chem. Eng.*, **8**, 3 (2020).
24. K. Wang, Y. Mao, C. Wang, Q. Ke and M. Zhao, *Environ. Sci. Pollut. Res.*, **29**, 36075 (2022).
25. M. Menon and N. Pryds, *Adv. Energy Mater.*, **205**, 5 (2008).
26. F. A. Rodríguez, E. P. Rivero and I. González, *MethodsX*, **5**, 1613 (2018).
27. R. F. Yunus, Y. Zheng, K. G. N. Nanayakkara and J. P. Chen, *Ind. Eng. Chem. Res.*, **48**, 16 (2009).
28. I. S. AL-Jobouri, S. A. Dhahir and K. A. AL-Saade, *Am. J. Environ. Sci.*, **9**, 3 (2013).
29. R. W. Ricci, M. A. Ditzler Robert and L. P. Nestor, *J. Chem. Educ.*, **71**, 983 (1994).
30. A. Goyal, V. C. Srivastava and J. P. Kushwaha, *Chem. Eng. J.*, **325**, 289 (2017).
31. R. Chauhan, V. C. Srivastava and A. D. Hiwarkar, *J. Taiwan Inst. Chem. Eng.*, **69**, 106 (2016).
32. R. Chauhan and V. C. Srivastava, *Chem. Eng. J.*, **386**, 3 (2020).
33. H. Ajab, M. Hasnain and A. Yaqub, *Sust. Mater. Technol.*, **26**, e00225 (2020).
34. R. G. Freitas, L. F. Marchesi, R. T. S. Oliveira, F. I. Mattos-Costa, E. C. Pereira, L. O. S. Bulhões and M. C. Santos, *J. Power Sources*, **171**, 2 (2007).

35. E. Palma-Goyes, J. Vazquez-Arenas, C. Ostos, F. Ferraro, R. A. Torres-Palma and I. Gonzalez, *Electrochim. Acta*, **213**, 740 (2016).
36. R. Dixit and C. B. Majumder, *J. CO_2 Util.*, **26**, 80 (2018).
37. K. Rokosz, T. Hryniewicz and S. Raaen, *Tehnicki Vjesnik*, **22**, 1 (2015).
38. E. A. Paoli, F. Masini, R. Frydendal, D. Deiana, C. Schlaup, M. Malizia, T. W. Hansen, S. Horch, I. E. L. Stephens and I. Chorkendorff, *Chem. Sci.*, **6**, 190 (2015).
39. I. M. D. Gonzaga, A. R. Dória, V. M. Vasconcelos, F. M. Souza, M. C. dos Santos, P. Hammer, M. A. Rodrigo, K. I. B. Eguiluz and G. R. Salazar-Banda, *J. Electroanal. Chem.*, **874**, 114460 (2020).
40. S. J. Han, J. H. Song, J. Yoo, S. Park, K. H. Kang and I. K. Song, *Int. J. Hydrogen Energy*, **42**, 5886 (2017).
41. J. J. Pietron, M. B. Pomfret, C. N. Chervin, J. W. Long and D. R. Rolison, *J. Mater. Chem.*, **22**, 5197 (2012).
42. J. Zhou, T. Wang, C. Cheng, F. Pan, Y. Zhu, H. Ma and J. Niu, *Nanoscale*, **14**, 3579 (2022).
43. A. Kumar and B. Prasad, *Sep. Purif. Technol.*, **279**, 119677 (2021).
44. J. Zhou, T. Wang, C. Cheng, F. Pan, Y. Zhu, H. Ma and J. Niu, *Nanoscale*, **14**, 9 (2022).
45. M. Ahmadi, F. Vahabzadeh, B. Bonakdarpour, E. Mofarrah and M. Mehranian, *J. Hazard. Mater.*, **123**, 18795 (2005).
46. P. A. J. Rosa, A. M. Azevedo and M. R. Aires-Barros, *J. Chromatogr. A*, **1141**, 1 (2007).
47. Y. Hang, M. Qu and S. Ukkusuri, *Energy Build.*, **43**, 4 (2011).
48. R. Ghelich, M. R. Jahannama, H. Abdizadeh, F. S. Torknik and M. R. Vaezi, *Compos. Part B: Eng.*, **166**, 527 (2019).
49. M. Kumari and S. K. Gupta, *Sci. Rep.*, **9** (2019).
50. D. S. Ken and A. Sinha, *J. Environ. Chem. Eng.*, **9**, 1 (2021).
51. G. Villafane V. Bazán, E. Brandalez, A. López, P. Pacheco and A. Maratta, *Talanta Open*, **6**, 100149 (2022).
52. M. Tripathi, A. Bhatnagar, N. M. Mubarak, J. N. Sahu and P. Ganesan, *Fuel*, **277**, 118184 (2020).
53. R. E. Palma-Goyes, F. L. Guzmán-Duque, G. Peñuela, I. González J. L. Nava and R. A. Torres-Palma, *Chemosphere*, **81**, 1 (2010).
54. H. Ma, B. Wang and X. Luo, *J. Hazard. Mater.*, **149**, 2 (2007).
55. E. Chatzisymeon, N. P. Xekoukoulotakis, A. Coz, N. Kalogerakis and D. Mantzavinos, *J. Hazard. Mater.*, **137**, 2 (2006).
56. D. Ozturk, E. Dagdas, B. Ali Fil and M. J. K. Bashir, *Environ. Technol. Innov.*, **21**, 101264 (2021).
57. A. Sánchez-Sánchez, M. Tejocote-Pérez, R. M. Fuentes-Rivas, I. Linares-Hernández, V. Martínez-Miranda and R. M. G. Fonseca-Montes de Oca, *Int. J. Photoenergy*, **2018** (2018).
58. S. Singh, V. Kumar, N. Upadhyay and J. Singh, *J. Environ. Chem. Eng.*, **4**, 3 (2016).
59. B. K. Körbahti, K. Artut, C. Geçgel and A. Özer, *Chem. Eng. J.*, **173**, 3 (2011).
60. H. Khan, F. Wahab, S. Hussain, S. Khan and M. Rashid, *Chemosphere*, **291**, 132818 (2022).
61. L. Feng, J. Liu, Z. Guo, T. Pan, J. Wu, X. Li, B. Liu and H. Zheng, *Sep. Purif. Technol.*, **285**, 120314 (2022).
62. H. S. Awad and N. A. Galwa, *Chemosphere*, **61**, 9 (2005).
63. R. Kaur, J. P. Kushwaha and N. Singh, *Sci. Total Environ.*, **677**, 4 (2019).
64. A. A. Elbatea, A. Nosier, A. A. Zatout, I. Hassan, G. H. Sedahmed, M. H. Abdel-Aziz and M. A. El-Naggar, *J. Water Process Eng.*, **41**, 102042 (2021).
65. P. Asaithambi, M. B. Yesuf, R. Govindarajan, N. M. Hariharan, P. Thangavelu and E. Alemayehu, *Sep. Purif. Technol.*, **233**, 115935 (2019).
66. F. Ghanbari and M. Mahsa, *J. Environ. Chem. Eng.*, **3**, 1 (2015).
67. R. Patidar and V. C. Srivastava, *Chem. Eng. J.*, **403**, 125736 (2020).
68. A. E. Kuleyin, A. Gok and F. Akbal, *J. Environ. Chem. Eng.*, **9**, 104782 (2021).
69. S. Hussain, H. Khan, N. Khan, S. Gul, F. Wahab, K. I. Khan, S. Zeb, S. Khan, A. Baddouh, S. Mehdi, A. F. Maldonado and M. Campos, *Environ. Technol. Innov.*, **22**, 101509 (2021).
70. R. G. Rice, *J. Int. Ozone Assoc.*, **21**, 2 (2008).
71. K. E. O'Shea and D. D. Dionysiou, *Phys. Chem. Lett.*, **3**, 15 (2012).
72. M. P. D. Silva, A. C. A. Souza, L. E. Lima Ferreira, L. M. P. Neto, B. F. Nascimento, C. M. B. Araújo, T. J. M. Fraga, M. A. M. Sobrinho and M. G. Ghislandi, *Environ. Adv.*, **4**, 100064 (2021).
73. T. J. M. Fraga, M. P. Silva, E. M. P. L. Freire, L. C. Almeida, M. A. M. Sobrinho, M. G. Ghislandi and M. N. Carvalho, *Chem. Eng. Res. Des.*, **180**, 109 (2022).
74. L. M. S. Farias, M. G. Ghislandi, M. F. de Aguia, D. B. R. S. Silva, A. N. R. Leal, F. A. O. Silva, T. J. M. Fraga, C. P. de Melo and K. G. B. Alves, *Mater. Chem. Phys.*, **276**, 125356 (2022).
75. M. P. D. Silva, M. Z. S. B. Souza, J. V. F. L. Cavalcanti, T. J. M. Fraga, M. A. M. Sobrinho and M. G. Ghislandi, *Environ. Sci. Pollut. Res.*, **28**, 23648 (2021).
76. B. Sari, H. Güney, S. Türkeş and O. Keskinkan, *J. Int. Ozone Assoc.*, 1 (2022).
77. R. Chauhan and V. C. Srivastava, *Ind. Eng. Chem. Res.*, **60**, 15 (2021).
78. R. Chauhan and V. C. Srivastava, *Process Saf. Environ. Protect.*, **147**, 245 (2021).
79. R. Patidar and V. C. Srivastava, *Chem. Eng. J.*, **403**, 125736 (2020).
80. N. N. Drouiche, N. Ghaffourb, H. Lounicic, N. Mameric, A. Maallemia and H. Mahmoudid, *Desalination*, **223**, 1 (2008).
81. N. Kishimoto, T. Kitamura, M. Kato and H. Otsu, *Water Res.*, **47**, 5 (2013).
82. N. Mohan, N. Balasubramanian and C. A. Basha, *J. Hazard. Mater.*, **147**, 1 (2007).
83. H. Afanga, H. Zazou, F. E. Titchou, Y. Rakhila, R. Ait Akbour, A. Elmchaouri, J. Ghanbaja and M. Hamdani, *Sust. Environ. Res.*, **30**, 1 (2020).
84. A. S. Fajardo, H. F. Seca, R. C. Martins, V. N. Corceiro, I. F. Freitas, M. E. Quinta-Ferreira and R. M. Quinta-Ferreira, *J. Electroanal. Chem.*, **785**, 180 (2017).
85. L. Liang, L. Cheng, Y. Zhang, Q. Wang, Q. Wu, Y. Xue and X. Meng, *RSC Adv.*, **10**, 28509 (2020).
86. Q. Dai, L. Jiang and X. Luo, *Int. J. Electrochem. Sci.*, **12**, 4265 (2017).
87. H. Zhong, C. Sun, S. Yang, Y. Ding, H. He and Z. Wang, *J. Hazard. Mater.*, **162**, 1477 (2009).

Supporting Information

Rhodamine B dye degradation by fabricated Ti/RuO_2 anode: Optimization by RSM, reaction mechanism, study of sludge

Monica Ranga, Shishir Sinha†, and Pinakshi Biswas

Department of Chemical Engineering, Indian Institute of Technology Roorkee, Roorkee 247667, Uttarakhand, India
(*Received 16 August 2022 • Revised 19 November 2022 • Accepted 23 November 2022*)

Table S1. Increase in the weight of each layer of RuO_2 on Ti substrate after every deposition

Layers of RuO_2	Weight of Ti after deposition
1	4.1730
2	4.1863
3	4.1963
4	4.2010
5	4.2033
6	4.2126
7	4.2200
8	4.2269
9	4.2362

Table S2. Characteristics of dyeing unit wastewater before and after electrochemical process

Characteristics	Before treatment	After treatment
pH	8-10	-
Total suspended solids	32	10
COD (mg/l)	2,812	215
BOD (mg/l)	1,123	300
TOC (mg/l)	1,247	500
Total kjehdal nitrogen (TKN) (mg/l)	298	-

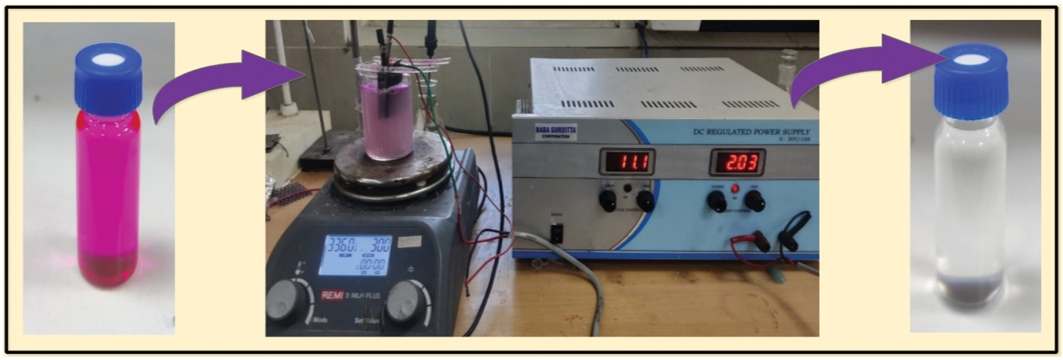


Fig. S1. Experimental setup of the electrochemical treatment process.

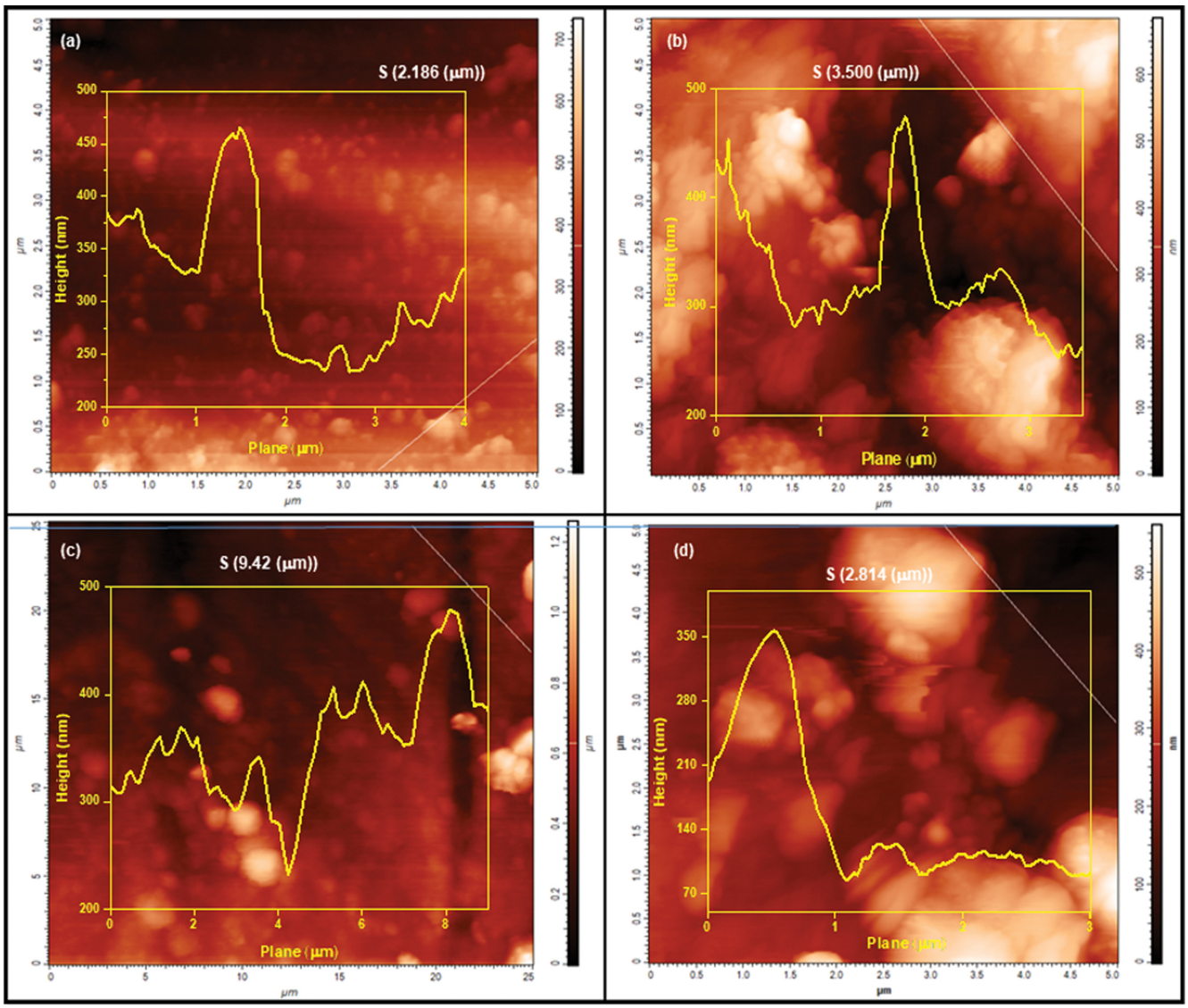


Fig. S2. 2D AFM images and their cross sectional analysis of the (a) Ti/RuO_2 before treatment (b) Ti/RuO_2 after treatment, (c) S.S. anode before treatment (d) S.S. after treatment.

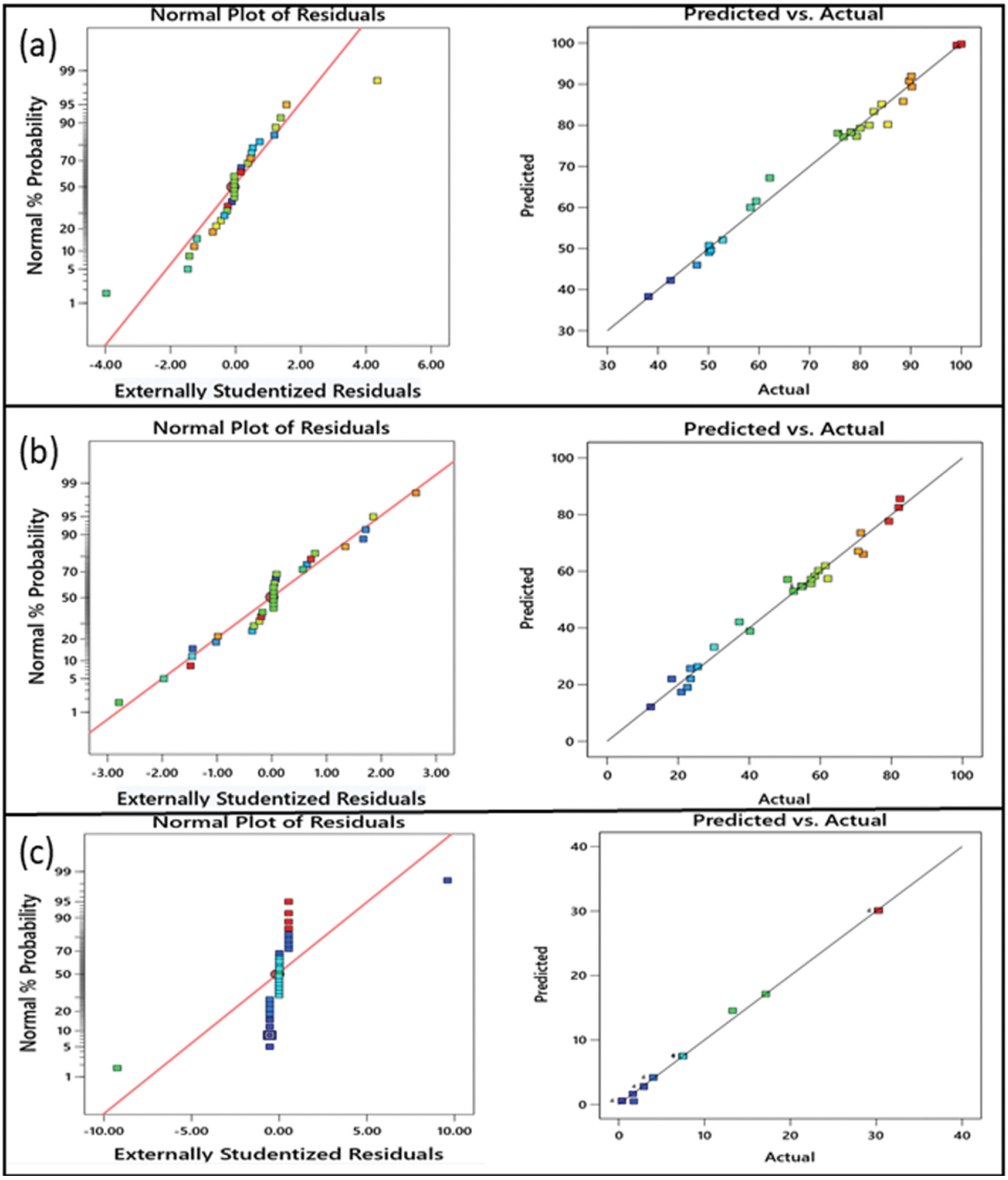


Fig. S3. Predicted vs Actual and their corresponding normal plots of residual for (a) % dye degradation (b) % COD removal (c) energy consumption.

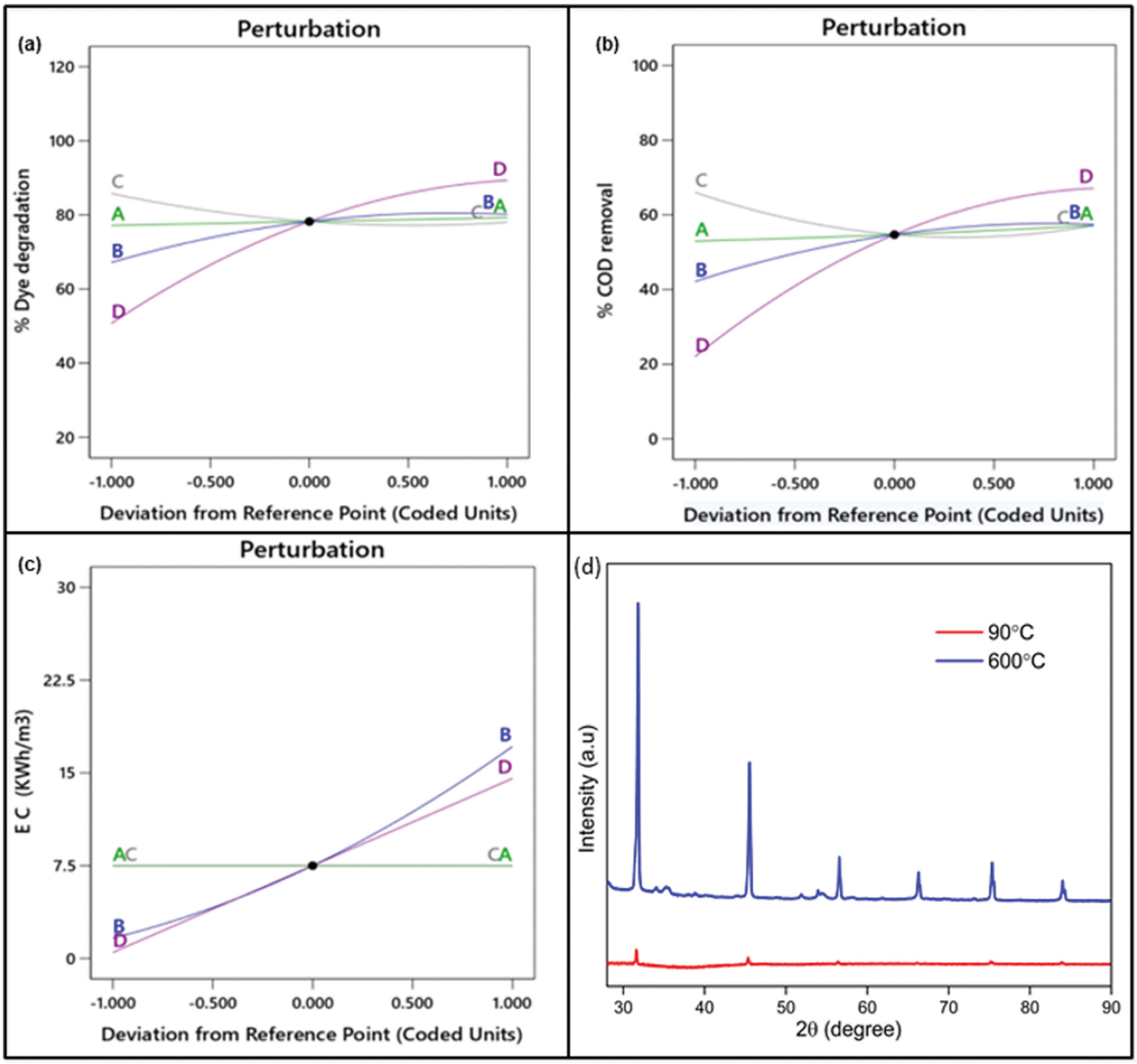


Fig. S4. Perturbation curve for (a) dye degradation, (b) COD removal, (c) energy consumption (A is pH, B is current, C is initial concentration, D is time) (d) XRD pattern sludge.

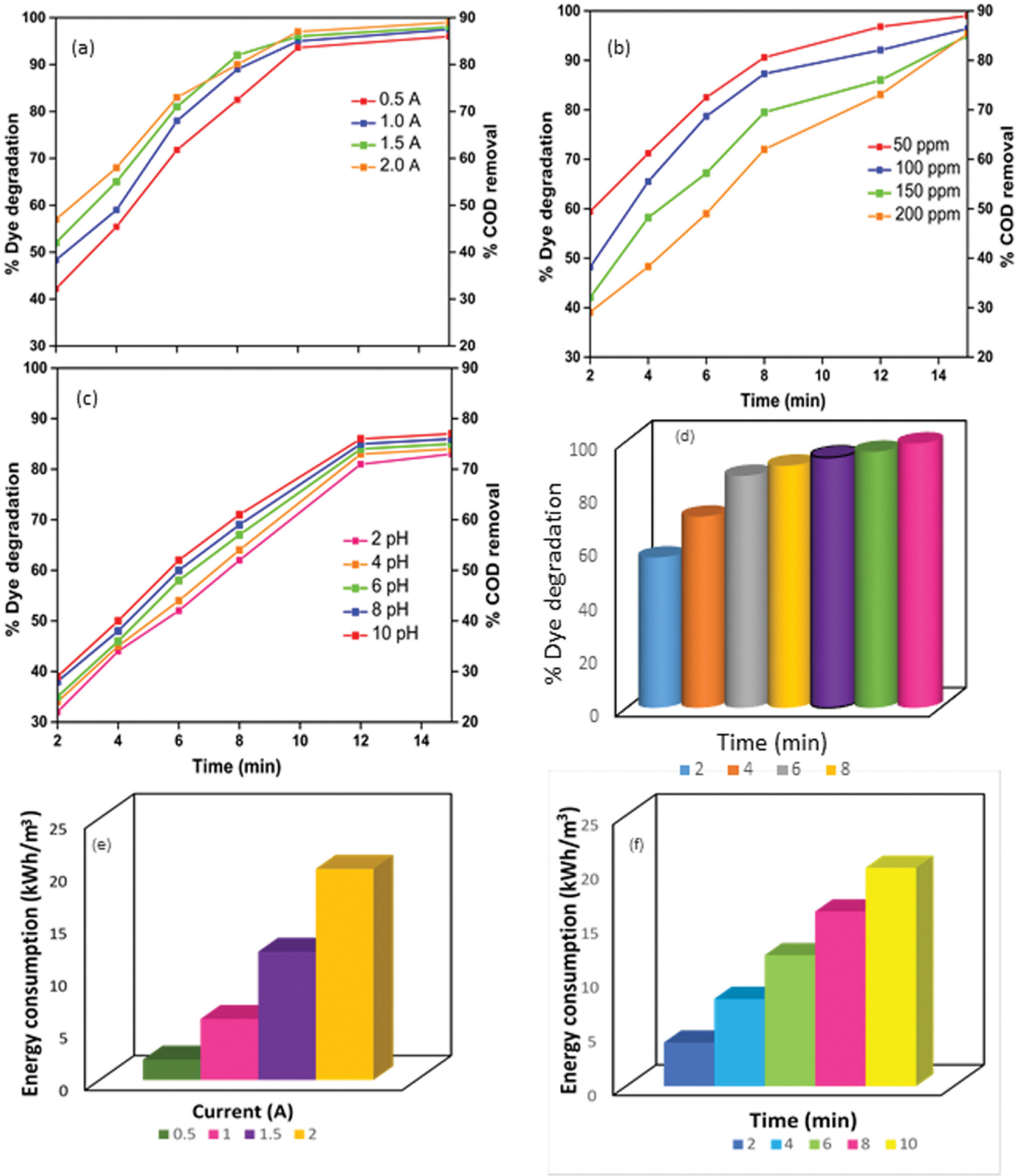
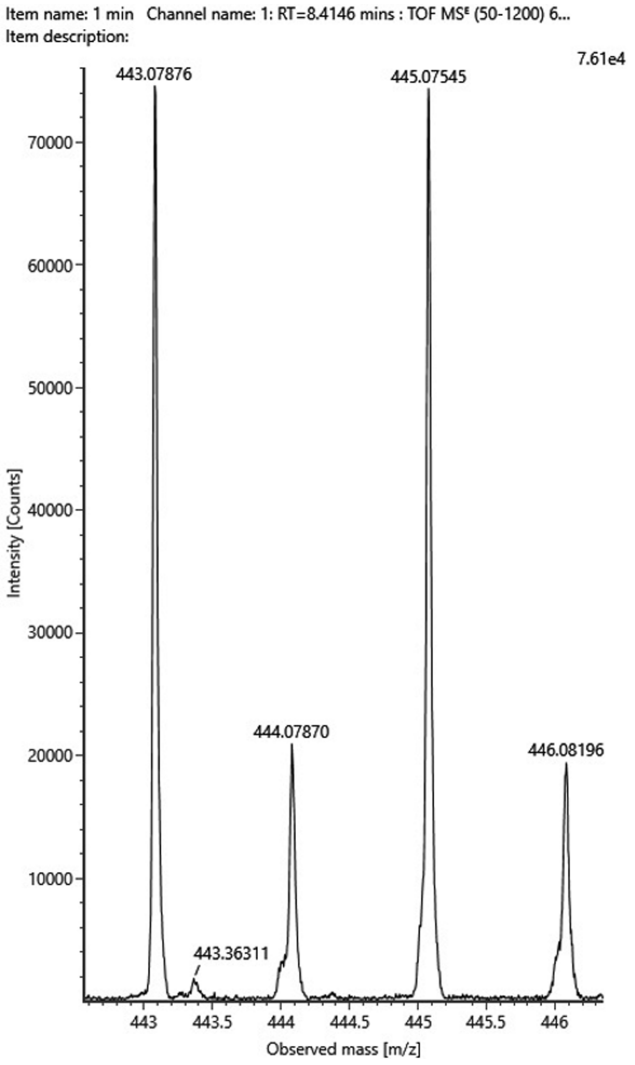
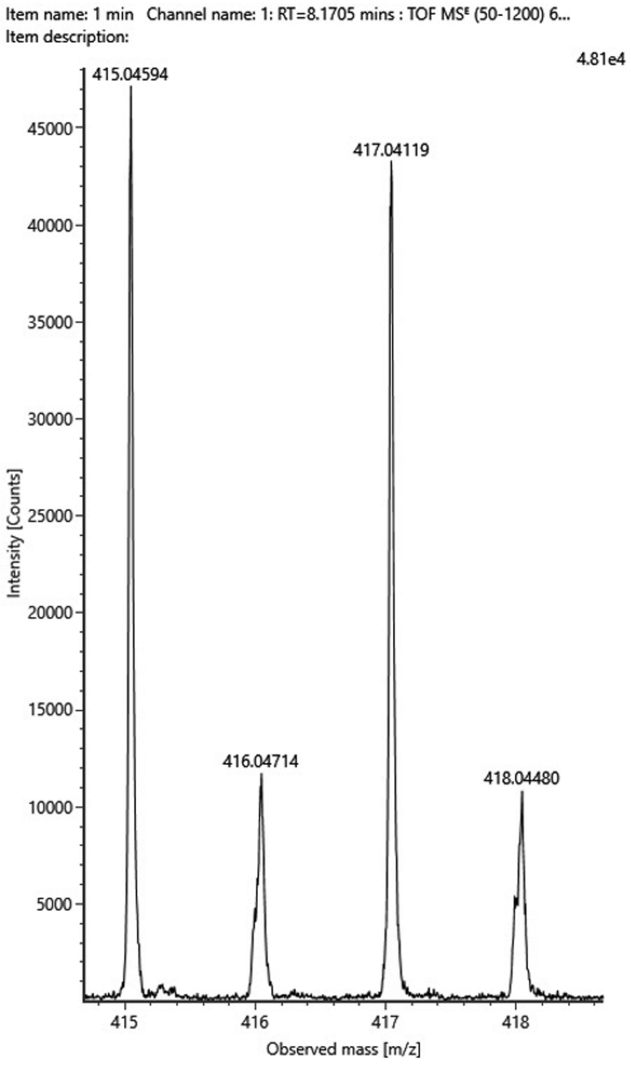
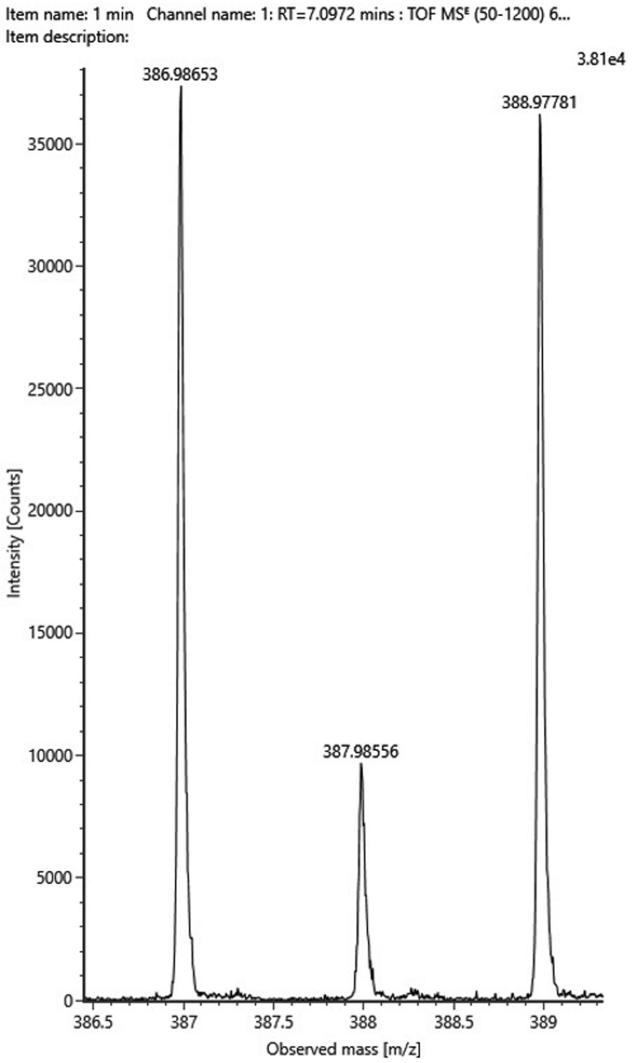


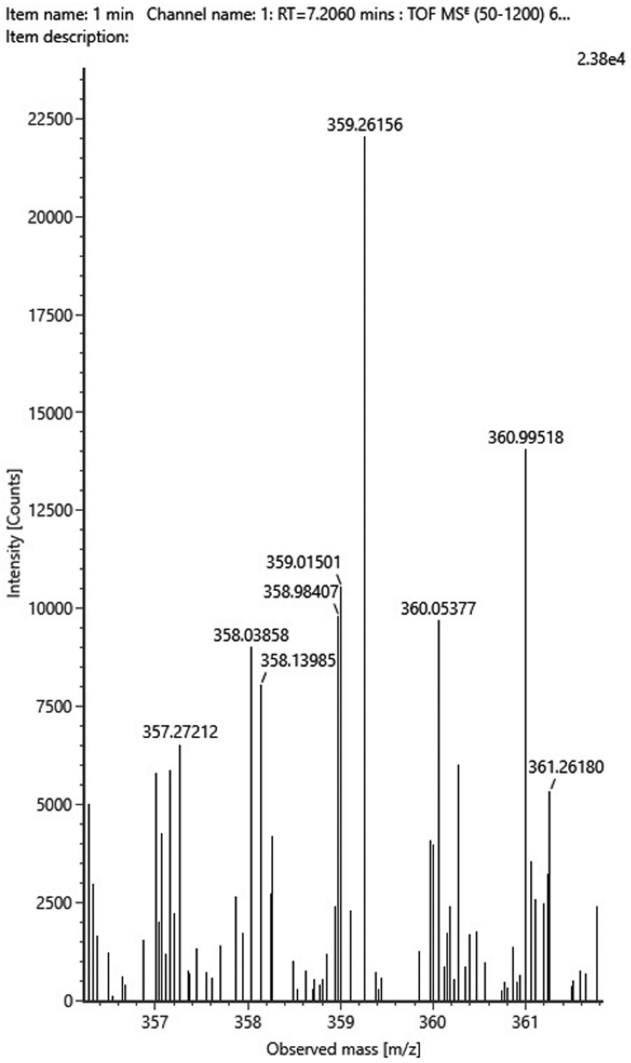
Fig. S5. Dye degradation and COD variation with (a) current (b) initial concentration (c) pH (d) dye degradation variation with time (e) energy consumption variation with current (f) energy consumption variation with time.

Table S3. Chromatographs of possible intermediates formed during the reaction

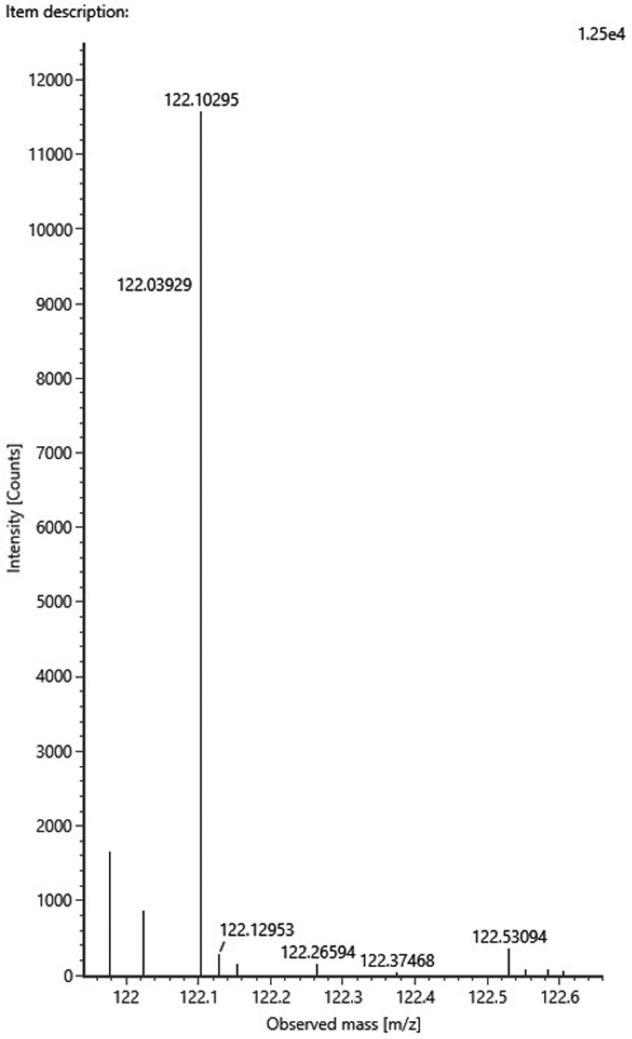





Item name: 1 min Channel name: 1: RT=7.0972 mins : TOF MS^E (50-1200) 6...
Item description:
3.81e4
386.98653
388.97781
387.98556
Intensity [Counts]
Observed mass [m/z]


Item name: 1 min Channel name: 1: RT=7.2060 mins : TOF MS^E (50-1200) 6...
Item description:
2.38e4
359.26156
360.99518
359.01501
358.98407
360.05377
358.03858
358.13985
357.27212
361.26180
Intensity [Counts]
Observed mass [m/z]

Item name: 1 min Channel name: 1: RT=6.3502 mins : TOF MS^{E} (50-1200) 6...
Item description:



Item name: 1 min Channel name: 1: RT=0.2176 mins : TOF MS^{E} (50-1200) 6...
Item description:

